



Dynamical downscaling of CMIP6 scenarios with ENEA-REG: an impact-oriented application for the Med-CORDEX region

Alessandro Anav^{1,2} · Marta Antonelli¹ · Sandro Calmanti¹ · Adriana Carillo¹ · Franco Catalano^{1,2} · Alessandro Dell'Aquila¹ · Roberto Iacono¹ · Salvatore Marullo¹ · Ernesto Napolitano¹ · Massimiliano Palma¹ · Giovanna Pisacane¹ · Gianmaria Sannino^{1,2} · Maria Vittoria Struglia^{1,2}

Received: 23 September 2023 / Accepted: 11 December 2023
© The Author(s) 2024

Abstract

In the framework of the coordinated regional modeling initiative Med-CORDEX (Coordinated Regional Climate Downscaling Experiment), we present an updated version of the regional Earth System Model ENEA-REG designed to downscale, over the Mediterranean basin, the models used in the Coupled Model Intercomparison Project phase 6 (CMIP6). The regional ESM includes coupled atmosphere (WRF), ocean (MITgcm), land (Noah-MP, embedded within WRF), and river (HD) components with spatial resolution of 12 km for the atmosphere, 1/12° for the ocean and 0.5° for the river rooting model. For the present climate, we performed a hindcast (i.e. reanalysis-driven) and a historical simulation (GCM-driven) over the 1980–2014 temporal period. The evaluation shows that the regional ESM reliably reproduces the mean state, spatial and temporal variability of the relevant atmospheric and ocean variables. In addition, we analyze the future evolution (2015–2100) of the Euro-Mediterranean climate under three different scenarios (SSP1-2.6, SSP2-4.5, SSP5-8.5), focusing on several relevant essential climate variables and climate indicators for impacts. Among others, results highlight how, for the scenarios SSP2-4.5 and SSP5-8.5, the intensity, frequency and duration of marine heat waves continue to increase until the end of the century and anomalies of up to 2 °C, which are considered extreme at the beginning of this century, will be so frequent to become the norm in less than a hundred years under the SSP5-8.5 scenario. Overall, our results demonstrate the improvement due to the high-resolution air–sea coupling for the representation of high impact events, such as marine heat waves, and sea-level height.

Keywords Regional Earth system models · Mediterranean climate · Marine heatwaves · Sea level height · Med-CORDEX · Future scenario

1 Introduction

Although global climate models (GCMs) and Earth system models (ESMs) represent an important source of climate information for the regional scale, regional climate models (RCMs) allow to better represent the complex phenomena that emerge at higher resolutions, especially over regions of complex orography or with heterogeneous surface

characteristics, such as the Mediterranean basin (Doblas-Reyes et al. 2021). As matter of fact, the last IPCC (Intergovernmental Panel on Climate Change) Assessment Report (AR) acknowledged that regional climate information for impacts and risk assessment is increasingly robust and mature to feed climate services and impacts studies with the higher resolution they need (Ranasinghe et al. 2021). On the other hand, local information on climate change impacts produced by global models should be considered with some caution (Gualdi et al. 2013).

In the Mediterranean region, the climate is characterized by the interplay between midlatitude and subtropical circulation regimes (Tuel and Eltahir 2020) with strong local air–sea interactions that can substantially influence the regional climate and the Mediterranean Sea circulation (Somot et al. 2008, 2018; Artale et al. 2010). Moreover,

✉ Alessandro Anav
alessandro.anav@enea.it

¹ Italian National Agency for New Technologies, Energy and the Environment (ENEA), Rome, Italy

² ICSC Italian Research Center on High-Performance Computing, Big Data and Quantum Computing, Bologna, Italy

the Mediterranean basin is a well-known hot-spot region for climate change (Giorgi 2006; Tuel and Eltahir 2020; Cos et al. 2022) and, due to both its conformation and the distribution of the population over its territory, it is particularly vulnerable to both hydrogeological risks (heavy rainfall, landslides, flooding) and coastal risks (sea level rise, marine heat waves) with effects on the health and economies of communities. Hence, predicting the effects and extent of climate change over this region has important implications for natural ecosystems (Ciais et al. 2005; Richon et al. 2019; Pagès et al. 2020; Reale et al. 2022a) and millions of people already exposed to heat waves and water-stressed conditions (Michetti et al. 2022). Furthermore, understanding and predicting the effects of climate change allows to improve the methodologies for prevention, adaptation and mitigation strategies.

For these reasons, different regional climate models have been developed and used to study both present and future Mediterranean climate systems (e.g., Dubois et al. 2012; Ruti et al. 2016; Darmaraki et al. 2019; Parras-Berrocal et al. 2020; Soto-Navarro et al. 2020; Reale et al. 2022b) within a Coordinated Regional Climate Downscaling Experiment (CORDEX) protocol ensuring that model simulations are carried out under similar conditions (Giorgi and Gutowski 2015). Indeed, to be relevant and useful for decision-making, climate information must rely on multiple lines of evidence, based on ensembles of different models and on data-based process understanding (Doblas-Reyes et al. 2021).

In the framework of the CORDEX program, regional climate model simulations dedicated to the Mediterranean area belong to the Med-CORDEX initiative (Ruti et al. 2016). One of the objectives of this initiative is to better reproduce the intense air-sea interactions that characterize the Mediterranean region, by developing ocean-atmosphere coupled models aimed at improving the performance of local information at climatological scales and provide reliable future projections.

The ability of regional models to reliably reproduce the observed changes in mean and extreme temperature and precipitation over the Euro-Mediterranean region is widely documented (e.g. Kotlarski et al. 2014; Katragkou et al. 2015; Gutiérrez et al. 2021). In particular, hindcast (i.e. analyses-driven) experiments, conducted within the Euro-CORDEX (Jacob et al. 2014) and Med-CORDEX (Ruti et al. 2016) coordinated initiatives demonstrated the capability of reproducing both the main characteristics of Euro-Mediterranean climate and the local circulation features (Cardoso and Soares 2022; Drobinski et al. 2018) at resolutions ranging between 12 and 25 km (Kotlarski et al. 2014; Fantini et al. 2018). Furthermore, regional models provide improved resolution of the spatial patterns and seasonal cycles of precipitation, including extremes (e.g., Heikkilä et al. 2011; Giorgi and Gutowski 2015).

The results of these coordinated regional modelling initiatives have allowed the scientific community to define a number of climatic quantities that are relevant to socio-economic sectors and natural systems (Ranasinghe et al. 2021). Additionally, the Global Climate Observing System (GCOS—<https://gcos.wmo.int/en/home>) developed the concept of essential climate variables (ECVs), namely relevant parameters for the characterization of Earth's climate. ECVs can be either physical, chemical or biological, single or grouped (due to their joint concurrence in determining critical processes). They provide reliable, traceable, observation-based evidence that enables the accurate modeling and prediction that support policy development and adaptation planning, by helping scientists understand the drivers of past, current, and future climate variability (GCOS 2016). ECVs also provide a benchmark for climate model validation and guidance as to the essential variables that should constitute the standard output of any numerical experiment. Among ECVs, temperature and precipitation are known to affect a wide variety of processes and systems, with important consequences for natural ecosystems and human society.

Similarly, the Global Ocean Observing System (GOOS—<https://www.goosocean.org/>), defined a list of critical variables (Essential Ocean Variables, i.e. EOVs). Among EOVs, sea level height integrates several complex processes, whose interaction can dramatically affect coastal ecosystems and communities under a changing climate. The sea level rise under future scenarios represents a risk for people, coastal ecosystems, and infrastructure, particularly in the Mediterranean basin where millions of people live on coastal areas (Carrillo et al. 2012; Sannino et al. 2022). Similarly, rising Sea Surface Temperatures (SST) can also significantly affect the current equilibrium of our oceans, as well as several economic activities that traditionally exploit marine resources.

Within the Med-CORDEX initiative, we developed an improved version of the regional Earth system model ENEA-REG (Anav et al. 2021) specifically designed to downscale the models of the Coupled Model Intercomparison Project (CMIP) (Eyring et al. 2016) over the Mediterranean basin. Here we focus on the latest CMIP phase (i.e. phase 6, hereafter CMIP6) of the World Climate Research Programme (WCRP) initiative, aimed at improving our understanding of past, present and future climate changes related to natural variability and anthropogenic radiative forcing, in a multi-model framework.

In the following sections, we first assess the skills of ENEA-REG in reproducing present climate conditions in terms of relevant ECVs and EOVs. Validation is performed by comparing results from a historical simulation (i.e., regional ESM forced by global ESM simulation) with those of a hindcast experiment (i.e., regional ESM forced with reanalysis data) and a set of observational-based and reanalysis datasets to assess model performances and identify

possible shortcomings of the regional ESM. Then, we show climate projections under three different scenarios and, as an example of the added value for impact studies, we present an analysis of marine heatwaves in the simulated scenarios. In fact, the high-resolution coupling between the atmospheric and the oceanic model is expected to affect the behavior of extreme events implying energy and mass fluxes which are, at the same time, intense and localized geographically, particularly in the Mediterranean basin (e.g., Lebeaupin-Brossier et al. 2015). As marine heatwaves are expected to increase in frequency and intensity under climate change (Darmaraki et al. 2019), understanding their future occurrence under different climate scenarios is fundamental to assess the impacts on marine ecosystems and prevent financial losses associated to fish mortality.

2 Model description and experiment design

The ENEA-REG (Anav et al. 2021) is a regional ESM comprising multiple modeling components, namely the atmosphere, ocean, land, and river routing, designed for high-resolution climate studies and applications. The data exchange, regridding, and interpolation among model components are facilitated by the utilization of the RegESM coupler, as detailed in Turuncoglu (2019). RegESM is based on the Earth System Modeling Framework (ESMF) library, specifically version 7.1, and the NUOPC (National Unified Operational Prediction Capability) layer to establish interconnections, synchronization, and horizontal grid interpolation among the various model components.

ENEA-REG is based on the Weather Research and Forecasting (WRF version 4.2.2, Skamarock and Klemp 2008) to simulate the atmosphere dynamic, the Massachusetts Institute of Technology General Circulation Model (MITgcm version z67; Marshall et al. 1997) to represent the ocean state and circulation, while the Hydrological Discharge (HD version 1.0.2, Hagemann and Dümenil 1998; Hagemann and Gates 2001) model is used to simulate freshwater fluxes over the land surface and to provide a river discharge to the ocean model (Table 1).

Compared to the version described in Anav et al. (2021), here we use an updated WRF version that employs hybrid vertical levels instead of sigma-p vertical coordinates. Moreover, we have implemented the double-moment microphysics and cumulus parameterization proposed by Morrison et al. (2009) and Janjić et al. (1994), respectively. The main improvement in the ocean model is represented by the introduction of the full non-linear free-surface formulation (Campin et al. 2004). The ocean boundary conditions are consistently changed with the inclusion of monthly sea level fields. In addition, temperature and salinity profiles at the boundary are also prescribed as monthly means rather than

climatological values. The spatial-dependent horizontal viscosity is obtained from the turbulence closure scheme by Leith (1968). Leith's scheme focuses on resolving the direct enstrophy cascade (cascade towards the smaller scales) that is characteristic of 2D turbulence (Fox-Kemper and Menemenlis 2008). The selected tracer advection scheme is a third-order direct space–time flux limited scheme. As in Anav et al. (2021), Nile and Black Sea are prescribed as climatological monthly means, while the initial condition for the starting month (August) has been derived from the hindcast simulation performed using the previous version of the ocean model (Anav et al. 2021), after computing the monthly climatological averages for the temperature and salinity fields. A synthesis of the main physical parameterizations used in this study by the atmospheric and ocean components of the ENEA-REG is given in Table 1.

As in Anav et al. (2021), the atmospheric and the ocean model exchange sea surface temperature (SST), surface pressure, wind components, freshwater (evaporation–precipitation) and heat fluxes. Unlike the previous version, here the net heat flux is computed from net longwave, net shortwave, latent heat, and sensible heat fluxes, while we provide the shortwave radiation as a separate term able to penetrate the ocean. Furthermore, the hydrological model uses surface and sub-surface runoff, provided by WRF, to compute the river discharge and exchanges this field with the ocean component to close the water cycle. Table 2 summarizes the fields exchanged from the different model components. The coupling time step between the ocean and the atmosphere is set to 3 h, while the coupling with the hydrological model is set to 1 day.

The model domain covers the Med-CORDEX region, as shown in Fig. 1. The horizontal resolution of the atmospheric and ocean components is 12 km and $1/12^\circ$ (approximately 10 km) respectively, while the river routing model is implemented on a regular grid of 0.5° .

In this study we have performed a hindcast simulation initialized and forced through ERA5 (Hersbach et al. 2020) and ORAS5 (Zuo et al. 2019) reanalysis for the atmospheric and ocean components, respectively. In addition, an historical and three CMIP6 global scenario simulations (SSP1-2.6, SSP2-4.5, SSP5-8.5, Eyring et al. 2016; O'Neill et al. 2016) have been downscaled; in particular we have selected the CMIP6 MPI-ESM1-2-HR (Gutjahr et al. 2019) as driving model that is characterized by the following configuration: T127 (0.93° or ~ 103 km) for the atmosphere and TP04 (0.4° or ~ 44 km) for the ocean.

Among all the available CMIP6 models, in addition to the relatively high spatial resolution, we selected the MPI-ESM1.2-HR as it has a well-balanced radiation budget and its climate sensitivity is explicitly tuned to 3 K (Müller et al. 2018), making this model well suited for prediction and impact studies. Both the present-climate experiments

Table 1 Setup of the ENEA-REG system along with the main physical parameterizations used in this study by the atmospheric and ocean components

Atmosphere	
Model	WRF (v4.2.2)
Domain	Med-CORDEX
Horizontal resolution	12 km
Domain size	480×350 cells (lon x lat)
Vertical resolution	50 hybrid levels up to 10 hPa
Physical time step	60 s
Forcing	ERA5 (present) and MPI-ESM1-2-HR
Relaxation zone	10 points with an exponential relaxation
Microphysics	Morrison (two-moment scheme)
Cumulus parameterization	BMJ
Shortwave radiation	RRTMG
Longwave radiation	RRTMG
Land-surface model	NOAH-MP
Planetary boundary layer	YSU
Ocean	
Model	MITgcm (z67)
Domain	Mediterranean Sea
Horizontal resolution	1/12°
Domain size	570×264 cells (lon x lat)
Vertical resolution	75 z levels
Time step	150 s
Forcing	ORAS5 (present) and MPI-ESM1-2-HR
Relaxation zone	18 grid points
Vertical mixing	GGL90
Hydrology	
Model	HD
Resolution	0.5°
Time step	Daily
Driver	
Name	RegESM
Library	ESMF (v7.1)/NUOC

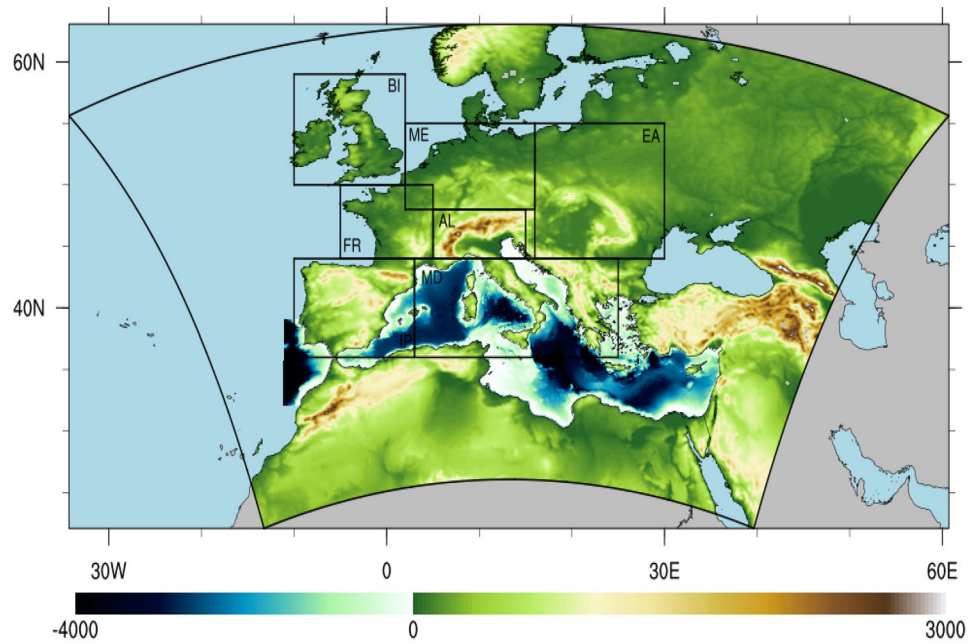
Note that, according to the Med-CORDEX protocol, Nile river discharge is prescribed to a climatological value. Similarly, the inflow of water from the Black Sea is parameterized as river with discharge values based on the monthly climatological net inflow rates available in Kourafalou and Barbopoulos (2003)

Table 2 List of the variables exchanged through the RegESM coupler between the different model components

Field	From	To	Notes
Sea surface temperature	MITgcm	WRF	Temperature at first ocean model level
Zonal wind	WRF	MITgcm	–
Meridional wind	WRF	MITgcm	–
Freshwater flux	WRF	MITgcm	Given as evaporation minus precipitation
Solar heat flux	WRF	MITgcm	Downward shortwave radiation considered as penetrative component of the air-sea heat flux
Non-solar heat flux	WRF	MITgcm	Non-penetrative component of the air-sea heat flux computed from longwave radiation, sensible and latent heat fluxes
Atmospheric surface pressure	WRF	MITgcm	–
Surface runoff	WRF	HD	From the NOAH-MP land model
Subsurface runoff	WRF	HD	From the NOAH-MP land model
Discharge at the river mouth	HD	MITgcm	Remapped and spread over the MITgcm gridpoints

The coupling time step between the ocean and the atmosphere is set to 3 h, while the coupling with the hydrological model is set to 1 day

Fig. 1 Domain used for the ENEA-REG simulations; the area defined by the black solid line represents the computational domain of the atmospheric model, with green shading highlighting the topography. The ocean domain is defined by the blue shading, used to represent bathymetry. Black boxes indicate seven regions, defined in the frame of the PRUDENCE project (Christensen and Christensen 2007), which are widely used for evaluation of climate models over Europe; they are: the Alps (AL), the British Isles (BI), Eastern Europe (EA), France (FR), the Iberian Peninsula (IP), the Mediterranean (MD), and Mid-Europe (ME).



cover the period 1st August 1980–31st December 2014, while future climate simulations span the period 2015–2100.

In general, ESMs exhibit various biases when compared to observations (Gleckler et al. 2008); thus, when forcing a regional climate model with a global model, these biases could propagate into regional simulations originating some regional biases and contributing to the uncertainties of climate projections (Dosio 2016). To overcome this problem, several bias correction techniques can be applied to the forcing data before using them for the dynamical downscaling. Here, we do not perform any bias correction to the high frequency lateral boundary conditions (i.e., 6 h) of the MPI-ESM1-2-HR atmospheric component, while monthly salinity, temperature and elevation used as open boundary conditions for the MITgcm model are bias-corrected.

This different approach among ocean and atmospheric variables is due to the peculiar Mediterranean thermohaline circulation, which is extremely sensitive to the variations of temperature and salinity fields, even those penetrating from the lateral boundary conditions through the narrow Gibraltar Strait (Pinardi and Masetti 2000). Thus, in order to avoid any incorrect or unrealistic evolution of the Mediterranean circulation, induced by a spurious heat and salt content coming from the biased CMIP6, it is advisable to remove the bias of the forcing data (Med-CORDEX protocol, <https://zenodo.org/record/8210985>), considering also that an altered Mediterranean Sea circulation, caused by the poor quality of the lateral boundary conditions, could not be easily recovered through different a-posteriori bias correction techniques of the simulated marine fields.

The bias correction applied to the ocean variables follows the approach proposed by Bruyère et al. (2014) which

corrects the mean bias of the driving model keeping the original interannual variability and trends. Following this approach, the monthly data are decomposed into a mean seasonally varying climatological component (\overline{ESM}) plus a perturbation term (ESM') that includes both high-frequency variability and climate-change trends:

$$ESM = \overline{ESM} + ESM' \quad (1)$$

Similarly, the ORAS5 reanalysis data are broken down into a seasonally varying mean climatological component (\overline{Obs}) and a perturbation term (Obs'):

$$Obs = \overline{Obs} + Obs' \quad (2)$$

The present-climate and future bias-corrected MPI-ESM1-2-HR boundary conditions (ESM^{bc}) are then constructed by replacing the climatological mean from Eq. 1 with the climatological mean of the reanalysis computed from Eq. 2:

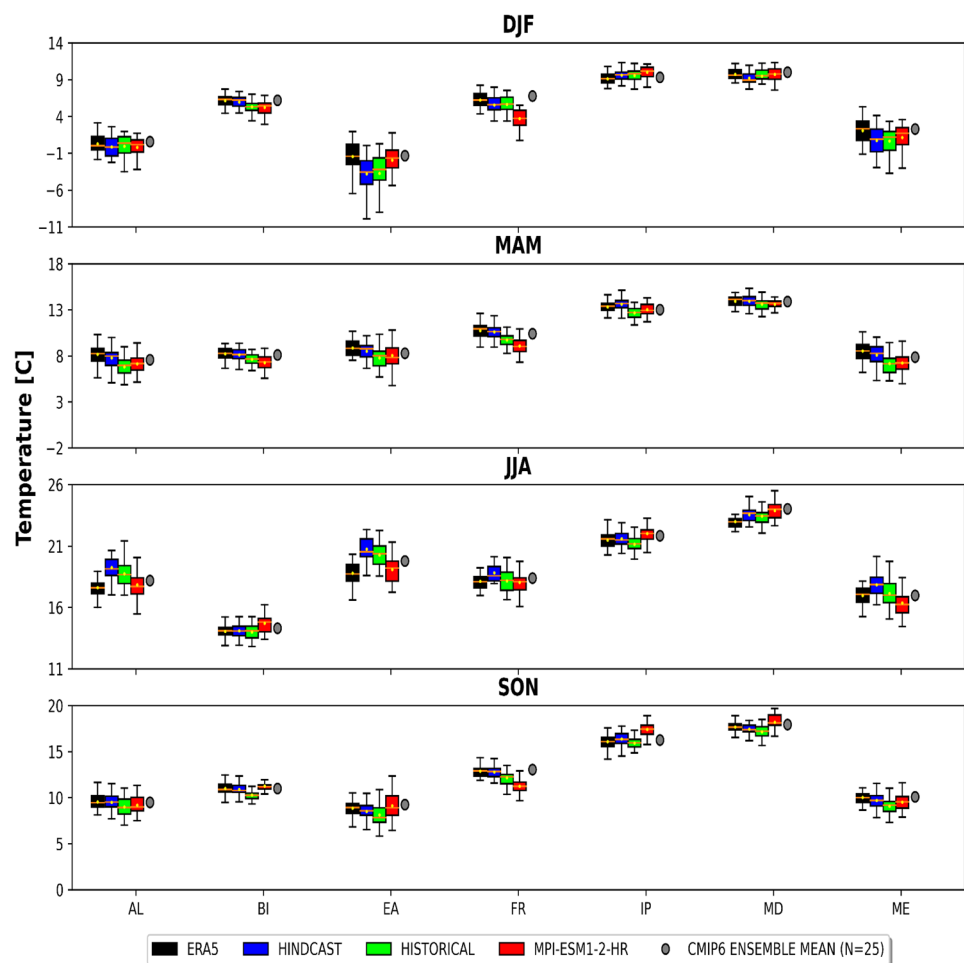
$$ESM^{bc} = \overline{Obs} + ESM' \quad (3)$$

3 Validation of ENEA-REG components

3.1 Present climate representation as simulated by the atmospheric model

To analyze the performance of the regional ESM in reproducing the mean annual cycle of surface air temperature, in Fig. 2 we compare box plots of seasonal mean temperatures from the hindcast and historical ENEA-REG downscaling

Fig. 2 Mean seasonal (winter, spring, summer, and fall) near-surface air temperature spatially averaged over the PRUDENCE regions from: reference data (ERA5, black boxes), the ENEA-REG hindcast (blue boxes) and historical simulations (green boxes), the driving model of the historical experiment (i.e. MPI-ESM1-2-HR, red boxes) and the ensemble mean of 25 CMIP6 models (gray circle). The orange lines within the boxes represent the median of the temperature while the yellow circles are used to indicate the mean value. The seasonal averages are computed over the period 1982–2014



experiments with ERA5 data. Although ERA5, like other reanalysis, is not entirely based on observations, it is widely used for validation of climate models, especially when used as forcing for downscaling experiments, since it allows to assess the model's ability to reliably reproduce the parent data (Mooney et al. 2013).

In the following analysis, in addition to the temperature simulated by the regional model, we also show the driving model (MPI-ESM1.2-HR) and the ensemble mean of 25 CMIP6 ESMs. Means, medians, and percentiles, computed for the temporal period 1982–2014, are spatially aggregated over the different sub-domains employed for model diagnostics in the regional climate change project PRUDENCE (Christensen and Christensen 2007).

Results suggest that the downscaling experiments reproduce quite well the seasonal temperature climatology for most of the PRUDENCE regions, although some large biases are found in some domains and seasons. In particular, the largest differences between ENEA-REG and ERA5 occur during winter (DJF, December–January–February) in Eastern Europe (i.e., EA subdomain) where the model shows a cold bias (-2.3 °C) in both simulations. Such a cold bias has

already been reported in several studies where the authors described some flaws of the model in treating surface temperature in wooded and snow-covered areas (e.g., Mooney et al. 2013; García-Díez et al. 2015; Katragkou et al. 2015). As recently discussed by Varga and Breuer (2020), the cold bias in the snow-covered regions is mainly caused by an overestimation of snow depth, a result of excessive snowfall and too weak melting.

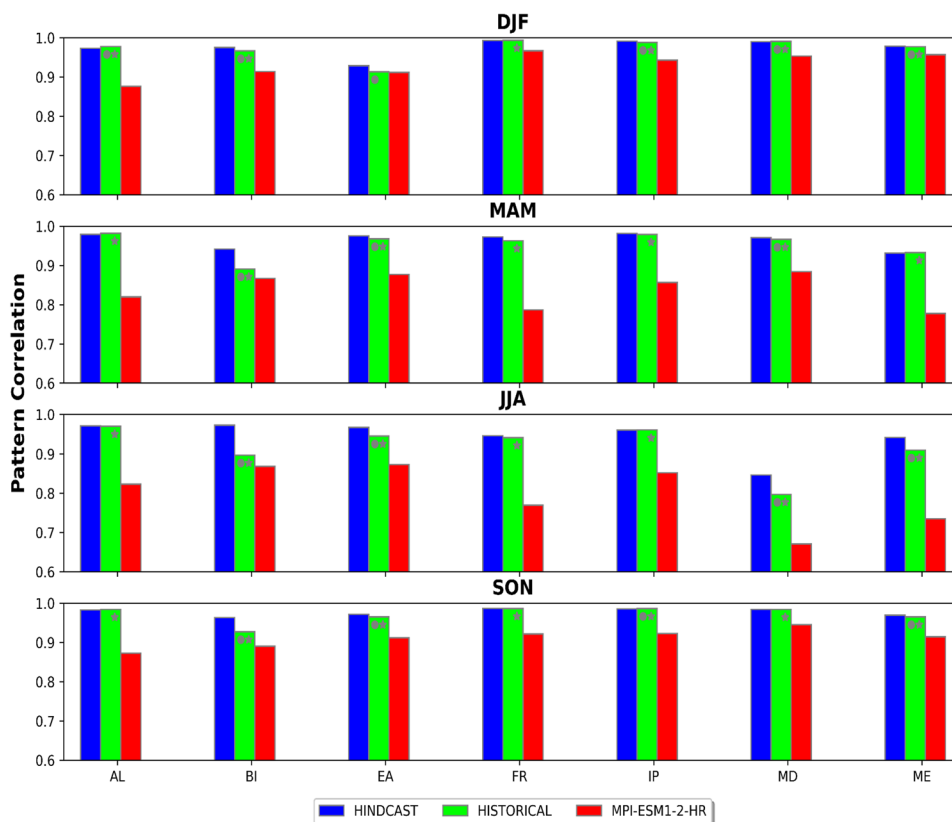
During summer (JJA, June–July–August) the downscaling experiments are systematically warmer than the reference data in several sub-domains with the most pronounced bias occurring in the Alpine region (1.6 °C in the hindcast and 1.1 °C for the historical) and over Eastern Europe (1.9 °C in the hindcast and 1.5 °C for the historical). Considering the other seasons, during spring (MAM, March–April–May) the hindcast simulation does not exhibit any relevant bias (maximum cold bias of 0.4 °C found in mid-Europe), while the historical simulation exhibits a cold bias larger than -1 °C in several sub-domains (i.e., Alps, Eastern Europe, France, and Mid-Europe). Similarly, in fall (SON, September–October–November) the hindcast simulation is in good agreement with reference data (the largest biases are found

over Eastern Europe – 0.4 °C and mid-Europe – 0.3 °C), while the historical experiment is systematically colder than ERA5 in all the sub-regions, with the larger bias occurring in mid-Europe (– 1 °C). In this latter case, the cold bias in these domains seems to be inherited by the driving MPI-ESM1.2-HR global model. Considering the CMIP6 models, it is widely known that, in terms of biases, the multi-model ensemble mean often outperforms most or all the individual ensemble members (e.g., Gleckler et al. 2008). Our results confirm that the CMIP6 ensemble mean is, in general, closer to ERA5 than the single MPI-ESM1.2-HR model. Noteworthy, in some regions (mostly in France, Iberian Peninsula and Mediterranean region) and seasons the MPI-ESM1.2-HR displays large bias compared to the reference data, while its downscaling performed with the ENEA-REG model is in good agreement with observations. This result confirms that coarse global models perform poorly over the complex-terrain regions surrounding the Mediterranean basin, while the downscaling of a global model produces more reliable results.

The spatial variability of surface temperature simulated by ENEA-REG is assessed by means of pattern correlations, computed over the PRUDENCE domains, using ERA5 as a reference (Fig. 3). Additionally, we have assessed the significance of pattern correlation difference between the historical and the hindcast simulations

(gray dot circles in Fig. 3) and between the historical and its driving global model (gray stars in Fig. 3). The null hypothesis of getting the same, or larger pattern correlation differences by chance, has been tested through a Monte Carlo bootstrap procedure with 1000 repetitions. The method is based on building synthetic data vectors by resampling with replacement the values of the two original series of grid points and computing quantiles on the vector of differences between the synthetic series (Wilks 2011). Results point out that the ENEA-REG historical and hindcast simulations are remarkably in agreement with ERA5 data for all the domains, while the pattern correlations of the MPI-ESM1.2-HR global model are always significantly lower, apart from EA in DJF. Besides, for several sub-domains and seasons, we found no significant differences in the spatial patterns of surface air temperature between the hindcast and historical simulations, while this latter is significantly better than its forcing. This result suggests that the spatial patterns are more dependent on local features and resolution than on the forcing used for the downscaling. This relevant improvement of the dynamical downscaling with respect to its driving ESM can be explained by the refinement of the spatial grid which is associated with a more realistic resolution of the non-homogeneous surface characteristics, like the land cover, the complex orographic features, and the land-sea contrast.

Fig. 3 Centered pattern correlation between the surface air temperature from the reference data (i.e. ERA5) and the ENEA-REG hindcast (blue boxes) and historical simulations (green boxes); besides, we also show the pattern correlation for MPI-ESM1.2-HR (red boxes) which has been used to drive the historical experiment. The seasonal patterns are computed for the reference period 1982–2014 over the PRUDENCE sub-regions (Christensen and Christensen 2007). In this analysis the two WRF experiments, and the global MPI-ESM1.2-HR model have been regridded to the ERA5 grid. 1% level significance of pattern correlation difference between the historical and the hindcast simulation (gray circles) and between the historical and the global model simulation (gray stars) has been assessed by bootstrap procedure with 1000 repetitions



Model performance in reproducing inter-annual variability has been assessed by the Model Variability Index (MVI, Gleckler et al. 2008); this metric provides a good measure to assess standard deviation differences between model and reference data and allows to identify areas with large biases in the magnitude of simulated variability. It is defined as:

$$\text{MVI} = \left(\frac{\sigma_o}{\sigma_m} - \frac{\sigma_m}{\sigma_o} \right)^2 \quad (4)$$

where the grid-point standard deviations of the model and the observations are indicated by m and o , respectively. The definition of a MVI threshold value that discriminates between “good” and “bad” is somewhat arbitrary (Anav et al. 2013): Scherrer (2011) suggested a threshold of 0.5 as a good representation of inter-annual variability, while when model variability equals that of the observations the MVI has a value of 0.

Seasonal MVI for the surface temperature (Fig. 4) shows how the hindcast well reproduces the observations variability

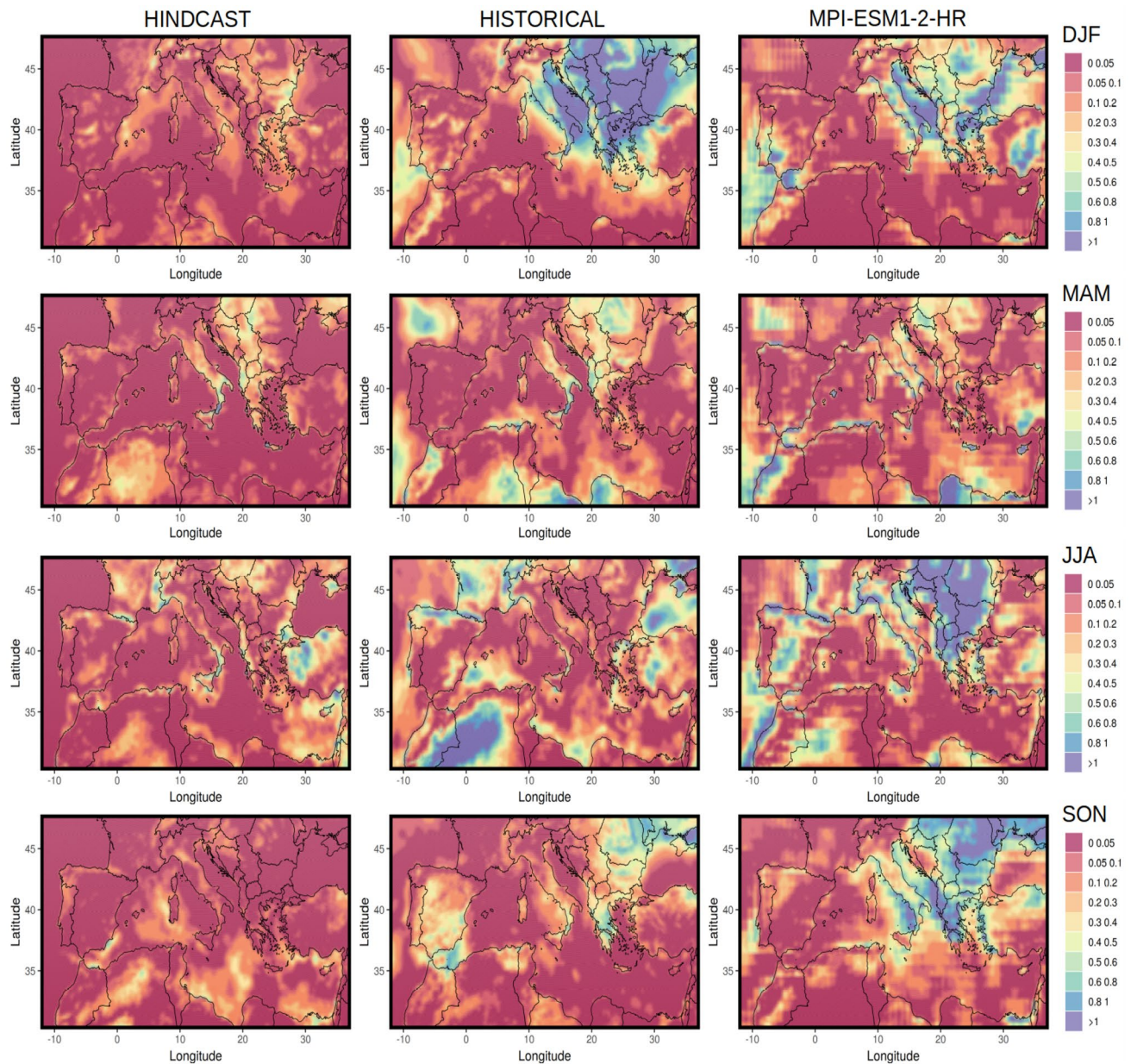


Fig. 4 Model Variability Index (MVI) of near-surface air temperature for the ENEA_REG hindcast simulation (left column), the ENEA-REG historical simulation (central column) and the MPI-ESM1-

2-HR simulation (right column). Boreal winter DJF (first row), spring MAM (second row), summer JJA (third row), autumn SON (fourth row)

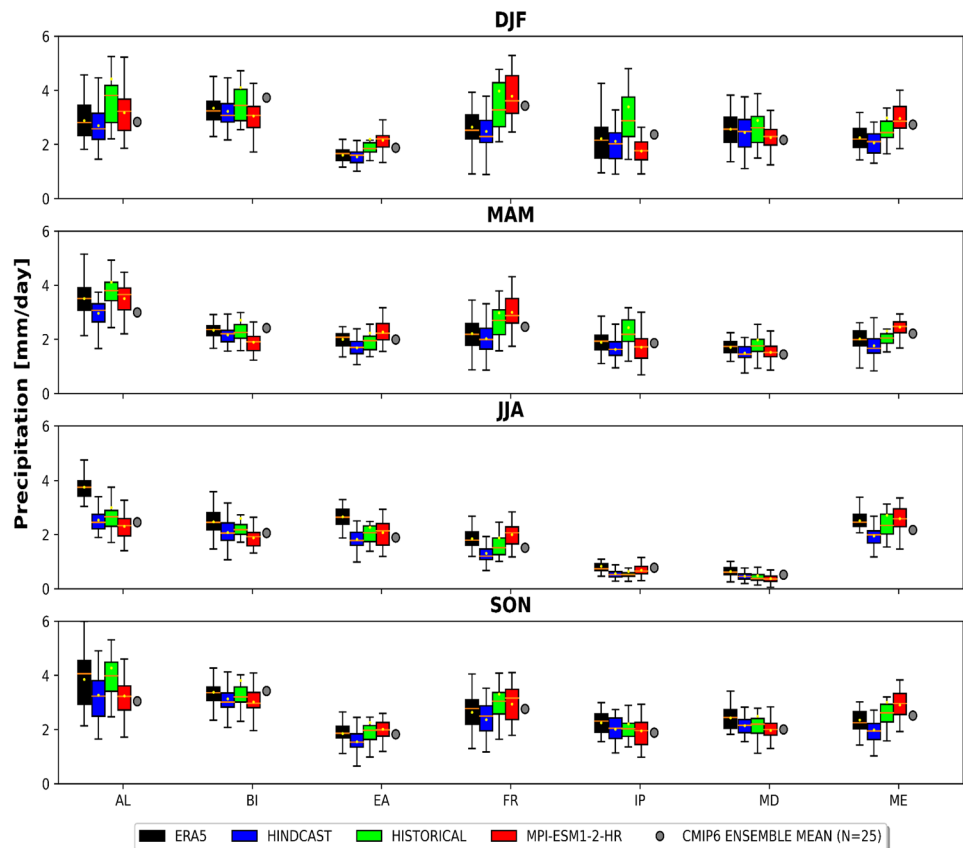
in all the seasons. Conversely, the historical simulation tends to inherit the variability reproduced by the global driving ESM, particularly in the seasons characterized by a strong influence of the synoptic conditions (coming from the forcing at the boundaries). On the other side, some improvements in MVI are evident over the Mediterranean region, particularly in JJA, when local circulations and small-scale processes are better resolved by the regional ESM than its driver, and during fall.

Looking at the Balkan region in DJF and Northern Africa in JJA, the historical simulation tends to amplify the interannual variability of the global forcing. As also in the hindcast simulation (see Figs. S.1, S.3, S.5 of supplementary material) these regions are characterized by an increase (within 30%) of the variability with respect to the ERA5 dataset, this suggests that the problem might be related to specific local processes' misrepresentation in the regional model. In particular, the common patterns over Africa could be attributed to differences between time-varying aerosols provided into ERA5 and the mean monthly climatology used in the ENEA-REG simulations (Pavlidis et al. 2020; Taranu et al. 2023). Similarly, considering the Balkan region, a possible explanation for the poorer MVI during winter could be related to the interplay between the well-known cold bias developing in the Eastern Europe (Fig. 2, Mooney et al.

2013; Katragkou et al. 2015; Anav et al. 2021) and the frequent North-Eastern outbreaks which transport cold air masses and hence increases the temperature variability over this region. As pointed out by Varga and Breuer (2020), this cold bias in winter is mainly caused by excessive snowfall and too persistent snow cover; as we found a common behavior between the historical and hindcast experiments (Fig. 2), the local snow-albedo-temperature feedback could play a crucial role to explain differences in temperature variability.

Consistent with the mean annual cycle of surface air temperature analysis, in Fig. 5 we compare box plots of seasonal mean precipitation from the two ENEA-REG downscaling experiments against ERA5 data. During winter we found the hindcast experiment in good agreement with ERA5 in all the sub-domains, with the largest dry bias of -0.2 mm/day occurring in the Alpine and Mediterranean region. On the other side, the historical run, except over the Mediterranean region, is systematically wetter than ERA5 and the largest biases are found over the Alps (1.5 mm/day), France (1.3 mm/day) and Iberian Peninsula (1.1 mm/day). Similarly, during MAM the hindcast is systematically drier than ERA5 in all the sub-domains (largest bias of -0.54 mm/day over Alps), while the historical is wetter and the largest discrepancies with respect to ERA5 are found over France (0.76 mm/day) and the Alps (0.6 mm/day). During

Fig. 5 As Fig. 2, but for precipitation



summer, the hindcast and historical simulations are generally drier than ERA5 with the largest biases found over the Alps for both the hindcast (-1.2 mm/day) and the historical (-0.75 mm/day). Finally, during SON the two downscaling experiments agree well with ERA5 in all the sub-regions and the most pronounced biases are found over the Alps in the hindcast (-0.58 mm/day) and over France (0.67 mm/day) in the historical. The driving MPI-ESM1.2-HR model displays a fairly good agreement with ERA5 data in most of the regions and seasons, with only France during winter, (1.1 mm/day) and Alps during summer (-1.4 mm/day) showing a bias larger than 1 mm/day.

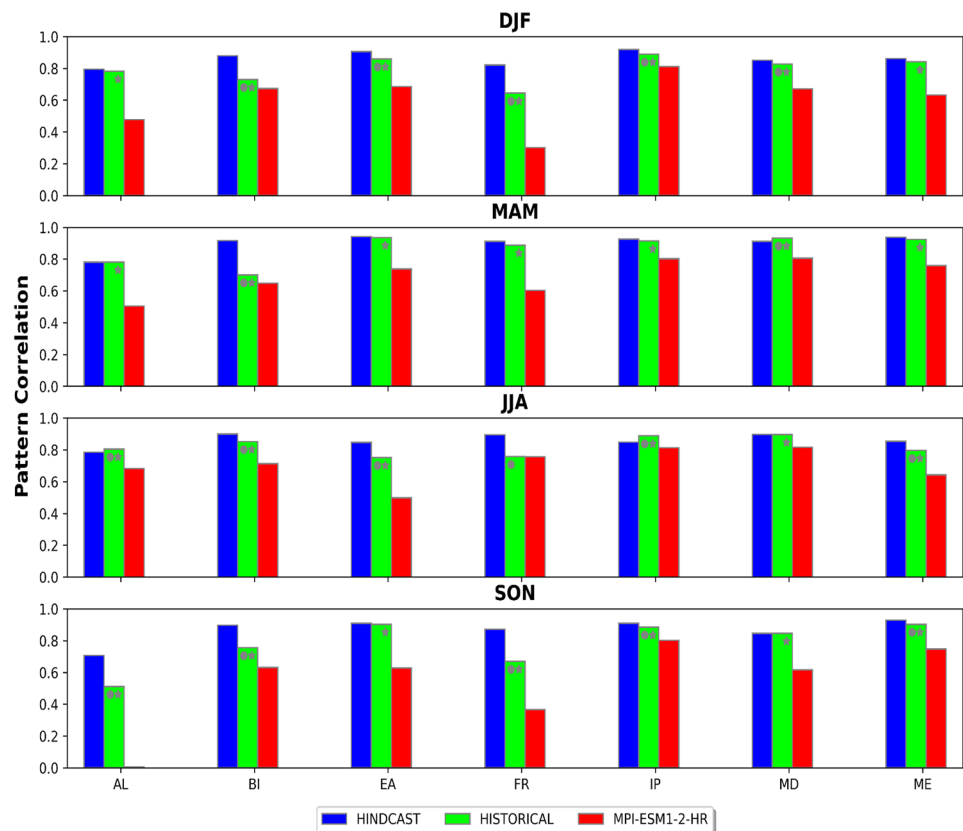
Figure 6 shows the pattern correlations for precipitation over the PRUDENCE domains. Results are consistent with those of surface temperature, although the displayed values are generally lower compared to those of Fig. 3. In general, the correlations show values around 0.8 and the poorest spatial agreement is found over the Alpine region for the historical experiment (0.5 during fall). Nevertheless, it is worth noting that in the same season and region the driving MPI-ESM1.2-HR model has a null correlation with respect to ERA5 data. Looking at the maps of precipitation (not shown), this discrepancy is caused by a spatial shift in rainfall patterns: specifically, the coarse global model simulates a large rainfall northern the Alps, while in the reanalysis the precipitation is more scattered around the mountains.

Besides, it is evident how results of the historical simulation are significantly different from MPI-ESM1.2-HR in all the regions and seasons (except France during JJA) and the downscaling substantially improves the spatial agreement with respect to ERA5.

The importance of improved resolution is particularly evident over the AL, EA and FR domains while the improvement of the spatial patterns of precipitation over the MD domain may be attributed also to the coupling with the high-resolution ocean model in ENEA-REG. This will be further discussed in Sect. 3.2.

Figure 7 shows the MVI of precipitation. Excluding summer, where the near-zero precipitation around the Mediterranean basin produces a MVI larger than 1, in all the remaining seasons we found a fair agreement between the downscaling experiments and ERA5. Unlike surface temperature, for precipitation the ENEA-REG tends to inherit the variability from the forcing for all the seasons. In particular, the areas where the historical simulation shows the larger MVI are the same where the global driving model has low performance. This is related to the resolution of the regional model (12 km) which is still not able to resolve the atmospheric convective structures (parameterized in our setup). Moving towards convection permitting resolutions is expected to significantly improve precipitation variability, especially in the summer season.

Fig. 6 As Fig. 3, but for precipitation



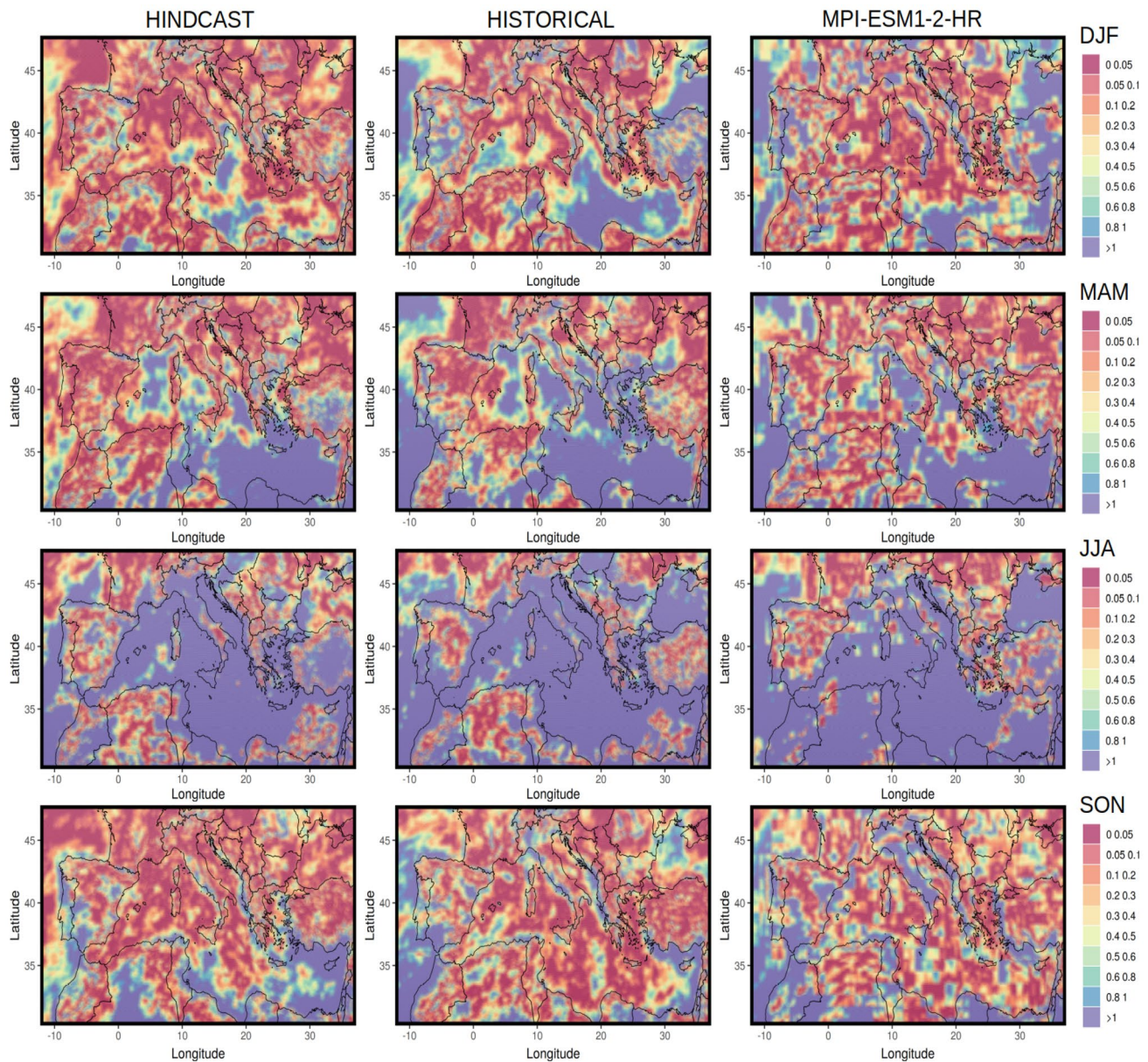


Fig. 7 Model Variability Index (MVI) of Precipitation for the ENEA-REG hindcast simulation (left column), the ENEA-REG historical simulation (central column) and the MPI-ESM1-2-HR simulation

(right column). Boreal winter DJF (first row), spring MAM (second row), summer JJA (third row), autumn SON (fourth row)

3.2 Present climate representation as simulated by the ocean model

In this section, we focus on the validation of the ocean component of ENEA-REG in terms of its capability of reproducing relevant fields, namely the EOVs, such as SST and sea level height, together with the surface circulation and the hydrological structure of the basin.

Considering the SST, we compare mean seasonal climatologies from the hindcast and historical ENEA-REG experiments with satellite-based observations

(SST_MED_SST_L4_REP_OBSERVATIONS_010_021); this latter is a daily, satellite retrieval reconstruction of SST, with a spatial resolution of 0.05° that is available through the portal of the Copernicus Marine Service (CMEMS; <https://marine.copernicus.eu/access-data>).

Figure 8 highlights a similar spatial distribution of the SST bias between the hindcast and the historical simulations, although this latter is systematically colder than the hindcast. Besides, both for the hindcast and for the historical run, the bias is positive during winter and negative in summer, implying a reduction in the amplitude of the seasonal

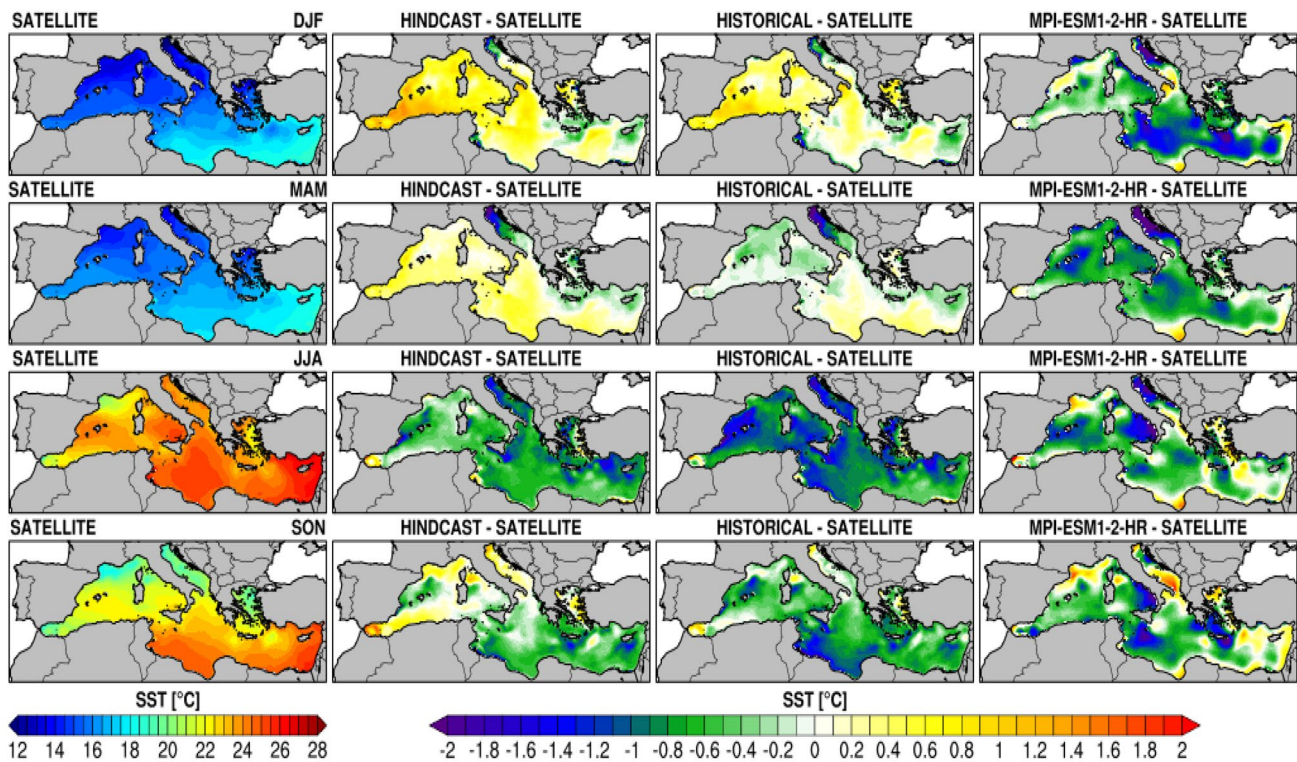


Fig. 8 Comparison of seasonal sea surface temperature from satellite data, the ENEA-REG hindcast and historical experiments and the MPI-ESM1-2-HR model. Seasonal averages are computed for the period 1982–2014

cycle of the downscaling experiments with respect to the observations. On the other side, the driving global ESM exhibits a less uniform pattern, with areas showing cold and warm biases during all the seasons; this is likely due to the insufficient representation of small-scale features which promotes large local differences with respect to satellite data.

Table 3 displays the vertical structure of temperature and salinity for the whole Mediterranean (MED) basin and its western and eastern sub-basins (WMED; EMED); here we show averages over three vertical layers (0–150 m, 150–600 m, 600–3500 m) for the reanalysis (MEDSEA_MULTYEAR_PHY_006_004 from the Copernicus Marine Service portal) as well as the associated biases of the hindcast and historical simulations. In general, the results are in good agreement with the reanalysis for both simulations. Considering the hindcast, it is warmer than the reanalysis, except for a small negative anomaly in the EMED upper layer, while the salinity is similar to the reference data in the western basin and slightly higher in the eastern. The historical simulation agrees well with the hindcast, with a slightly reduced bias in the western upper layer.

The average sea surface elevation and surface circulation, as simulated by the ENEA-REG, are compared to satellite observations obtained from the $1/8^\circ$ resolution Mean Dynamic Topography (MDT), which is representative of the

mean dynamic component. MDT is computed using satellite altimeter data and model results and is validated using independent observations (Rio et al. 2014). Figure 9 shows a close spatial agreement between the ENEA-REG and satellite observations, with the known permanent large-scale features well represented by the model. The overall representation of large mesoscale features is satisfactory, even though some anticyclonic anomalies in the Alborán Sea and in the Levantine are weaker than in the observations. In the Aegean Sea, however, and particularly in its northern part, both simulations display elevation anomalies smaller than in the observations; this local discrepancy will need to be further investigated.

Looking at the simulated mean circulation (Fig. 9), the hindcast and historical experiments show a similar spatial pattern suggesting that the ENEA-REG is able to capture all the main large-scale features of the geostrophic field already described in observation-based reconstructions (Millot and Taupier-Letage 2005) and other numerical studies (Pinardi et al. 2015; Anav et al. 2021; Sannino et al. 2022). The stream of Atlantic water (AW) entering from the Gibraltar Strait forms a meandering current along the North African coast, the Algerian Current, which bifurcates in proximity of the Sicily Channel. A weaker current bordering the Balearic Islands on the south side is also present in both experiments

Table 3 Average Temperature (°C) and Salinity (psu) at various depths for the whole Mediterranean (MED), the Western (WMED) and the Eastern (EMED) sub-basins

		Depth (m)		
		0–150	150–600	600–3500
		Temperature		
MED	Reanalysis	16.65	14.05	13.35
	Hindcast	0.09	0.25	0.27
	Historical	– 0.04	0.33	0.25
WMED	Reanalysis	15.41	13.46	12.96
	Hindcast	0.43	0.30	0.15
	Historical	0.15	0.25	0.13
EMED	Reanalysis	17.33	14.41	13.57
	Hindcast	– 0.08	0.21	0.36
	Historical	– 0.12	0.38	0.34
		Salinity		
MED	Reanalysis	38.41	38.82	38.66
	Hindcast	0.18	0.02	0.12
	Historical	0.15	0.04	0.11
WMED	Reanalysis	37.85	38.50	38.48
	Hindcast	0.04	0.04	0.03
	Historical	– 0.01	0.02	0.02
EMED	Reanalysis	38.73	38.85	38.81
	Hindcast	0.22	0.17	0.12
	Historical	0.22	0.21	0.12

The first-row reports averages from the Copernicus Reanalysis dataset, the second and third rows report differences between the hindcast and the historical simulations with respect to the reanalysis. All spatial averages are taken over the period 1987–2014

(Pinardi et al. 2015; Sannino et al. 2022) but is not clearly visible in the geostrophic reconstruction associated to the MDT. The two permanent cyclonic circulations that characterize the WMED, the wide gyre formed by the Liguro-Provençal current and the Bonifacio cyclone, are present in the simulations, and the two cyclonic structures occupying the central and southern portions of the Adriatic Sea (e.g. Palma et al. 2020, and therein references) are well resolved. It is worth stressing that the simulations correctly reproduce the circulation in the regions where deep and intermediate water formation takes place: the Gulf of Lion, the southern Adriatic, and the Levantine Sea.

Besides, the comparison of the annual time series of the average basin elevation from the hindcast with the observations (Fig. 9) suggests that the reanalysis-driven simulation captures the positive trend, the observed range of variation, and the main interannual variability in the period 1993–2014; nevertheless, a large discrepancy is found in the first years of the 2000s, a period characterized by strong atmospheric variability over the Mediterranean area, e.g. 2003 summer heat wave followed by a cold winter in 2004 (Mohamed et al. 2019).

3.3 Marine heat waves

Table 4 shows the performance of the ENEA-REG in reproducing the marine heatwaves in specific sites of interest around the Mediterranean basin; the test sites are defined as pseudo-rectangular areas of $1^\circ \times 1^\circ$ centered around the locations listed in Table 4.

Different operational definitions of marine heatwaves have been adopted in past studies, depending on the specific objectives. In general, heat waves should be characterized in terms of their duration, intensity, and spatial extent. A systematic, hierarchical approach to defining marine heat waves has been proposed by Hobday et al. (2016), who also introduced a specific taxonomy (symmetric, fast onset, slow onset, low intensity, high intensity). Following Hobday et al. (2016), the main features needed to define an heatwave are: (a) the identification of anomalies compared to a climatology referred to specific times of the year; (b) the length of the heatwave which is related to the specific process (e.g. ecological) of interest and (c) the possibility of identifying well defined start and end times.

In this study, we do not address any specific process or sectoral application, so we do not consider specific temperature thresholds or portions of the seasonal cycle particularly relevant for the analysis. Instead, we assume a general definition of heatwaves as periods of at least 5 consecutive days during which the mean temperature over a specific area of interest is above the long-term expected daily value (Hobday et al. 2016). For each test site we consider the areal mean of the daily surface temperature, and we apply singular spectrum analysis method (Allen and Smith 1997) to separate the slowest and smoothest components of the signal from the noisy and residual fluctuations on time scales ranging from a few days to less than six-months.

In doing so, the dependence on time is omitted and the sea surface temperature SST can be decomposed in the following terms:

$$SST = SST_C + SST_T + SST_S + SST_R \quad (5)$$

where SST_C is the mean temperature during the historical period, thus representing the current climate; SST_T is the long-term (i.e. multidecadal) trend component; SST_S is the periodic component of the signal, typically composed of a strong annual cycle and a weaker 6 months cycle which is likely associated to a phase shift of the different components of the total surface heat fluxes (Ruiz et al. 2008); SST_R represents the residual fluctuations on shorter time scales.

The first step in the assessment of the ENEA-REG performances in producing the heatwaves, is therefore to examine the distribution of the residuals by looking at the moments of their distribution in the case of the historical

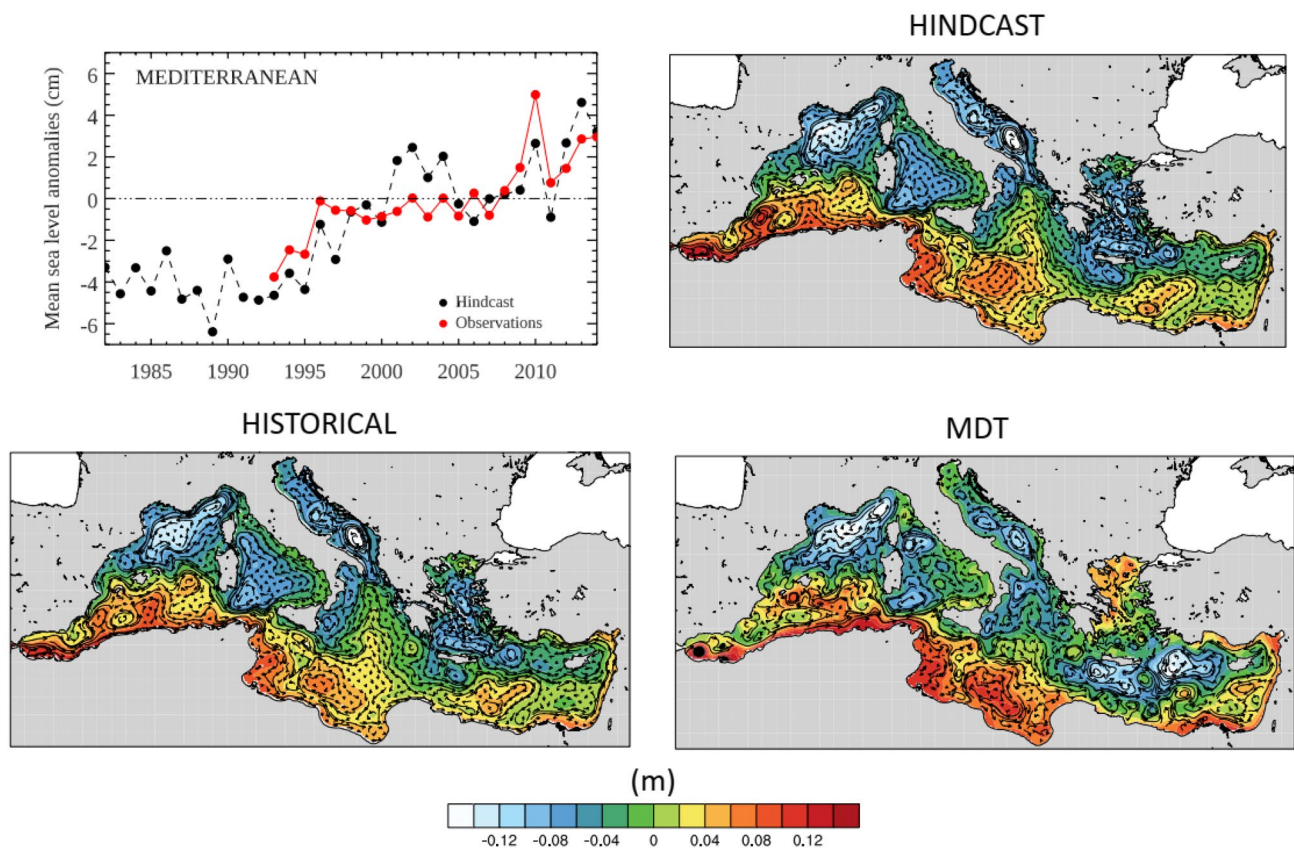


Fig. 9 The maps show the average sea level as simulated by the hindcast and historical experiments (1982–2014 average) and the satellite observations (1993–2014 average). The average circulation at 30 m of depth has been superimposed on the elevation in the two ENEA-REG simulations, while a geostrophic reconstruction of the circulation has

been used in the case of the MDT (also provided by CMEMS). In the top left panel, the annual time series of the average basin elevation from the hindcast (black dots) is compared with that resulting from the observations (red dots)

and hindcast simulations that can be directly compared with observation, as reported in Table 4.

For the mean, standard deviation and kurtosis there is no relevant improvement when comparing the global driver MPI-ESM1-2-HR with the regional climate model. Fluctuations are obviously distributed around a mean value of $0\text{ }^{\circ}\text{C}$ (not shown in Table 4) and both the regional and the global climate models tend to underestimate the standard deviation of the SST_R component. The average value of the kurtosis is slightly larger than 3 for all three datasets, implying a larger population of the tails of the distribution compared to normal distribution. However, no relevant differences emerge between the global driver and the regional downscaling compared to the observations.

Instead, more interesting, differences emerge when considering the skewness in the comparison between MPI-ESM1-2-HR, its regional downscaling with ENEA-REG and the corresponding hindcast simulation driven by ERA5. The skewness describes the asymmetries in the distribution of SST_R , whereby positive (negative) skewness implies a prevalence of warm (cold) anomalies in

the fluctuations. As a first example, in the Alboran Sea, the observed fluctuations are characterized by a slightly negative skewness ($-0.1\text{ }^{\circ}\text{C}$), and therefore by the prevalence of cold anomalies, which are likely linked to the ingression of relatively colder Atlantic waters into the Mediterranean, a feature of the oceanic circulation that the regional coupled model is able to capture whereas the global model does not have the appropriate spatial resolution to describe the process. In fact, while the skewness of the global driver is $0.3\text{ }^{\circ}\text{C}$ (prevalence of warm fluctuations), the historical simulation produces an improvement with a slightly negative skewness (approximated in Table 4 with $0\text{ }^{\circ}\text{C}$), whereas the hindcast has a skewness of $-0.2\text{ }^{\circ}\text{C}$.

Another interesting example is the case of the site north of Crete (CRETE-N) where MPI-ESM1-2-HR is characterized by an excess of cold fluctuation, likely associated to larger scale atmospheric winds blowing from the north, whereas the skewness for observations is $0.2\text{ }^{\circ}\text{C}$ (warm anomalies), correctly reproduced by the regional climate model, both in the hindcast and in the historical simulations.

Table 4 Standard deviation, skewness, and kurtosis of the distribution of the residual fluctuation (see Sect. 3.3 for a definition) of the average sea surface temperature over selected areas

	LON	LAT	Standard Deviation				Skewness				Kurtosis			
			OBS	HIN	MPI	HIS	OBS	HIN	MPI	HIS	OBS	HIN	MPI	HIS
ALBORAN	-3	36	0.9	0.6	0.7	0.6	-0.1	-0.2	0.3	0.0	4.0	3.8	4.6	3.6
LION	4	42	1.0	0.7	0.8	0.7	0.3	0.3	0.0	0.5	4.0	4.1	3.4	4.5
LIGURIAN	9	43.5	1.0	0.8	0.7	0.8	0.2	0.2	0.2	0.2	4.5	4.3	3.9	4.7
SICILY	11.5	38	0.8	0.7	0.6	0.6	0.1	0.0	0.3	0.3	3.5	4.3	3.9	3.9
TIRRENIAN	11.5	41	0.9	0.7	0.7	0.7	0.3	0.1	0.1	0.3	4.2	3.7	3.8	3.9
IONIAN-W	12.5	35.5	0.8	0.7	0.7	0.7	0.1	0.2	0.1	0.3	3.3	4.1	3.5	4.1
LAMPEDUSA	13	44.5	0.8	0.6	0.6	0.6	0.2	0.1	0.1	0.3	3.6	3.7	3.7	3.5
ADRIATIC-N	16.5	42.5	1.1	0.8	0.9	0.9	0.3	0.0	0.0	0.0	3.8	2.9	3.0	2.8
ADRIATIC-S	16.5	37	0.9	0.6	0.8	0.6	0.2	0.1	0.2	0.2	4.1	3.5	3.3	3.9
ADRIATIC-C	17	41.5	0.9	0.7	0.8	0.7	0.2	0.1	0.0	0.1	4.0	3.4	3.2	3.7
IONIAN-E	19.5	38.5	0.8	0.7	0.7	0.7	0.3	0.2	0.1	0.1	3.8	3.3	3.6	3.8
CRETE-N	24	36.2	0.8	0.5	0.7	0.6	0.2	0.1	-0.2	0.1	3.4	4.0	3.7	3.4
AEGEAN	24	34	0.9	0.6	0.8	0.6	0.0	0.0	0.1	0.1	3.7	3.7	4.0	3.5
CRETE-S	25	38.5	0.7	0.6	0.6	0.5	0.1	0.2	0.1	0.1	3.5	3.5	3.4	3.2
MARSA	27.5	32.5	0.6	0.5	0.7	0.5	-0.1	-0.1	0.1	0.0	3.3	3.1	3.1	3.3
RHODES	29	35	0.8	0.6	0.7	0.6	0.2	0.0	0.0	0.2	3.4	3.2	3.4	3.4
CYPRUS	32.5	33.5	0.7	0.5	0.7	0.5	0.0	0.2	0.0	0.2	3.3	3.1	3.0	3.1

Each area is defined as $1^\circ \times 1^\circ$ pseudo-rectangle centered around the coordinates indicated in the columns LON, LAT. OBS are the statistics derived from observations, HIN are the statistics from the hindcast simulation with ENEA-REG driven by ERA5, MPI is the historical simulation of the global model MPI-ESM1-2-HR and HIS is the historical ENEA-REG driven by MPI-ESM1-2-HR

Other local improvements can be highlighted in the Gulf of Lion, in the Tyrrhenian Sea and in the central Adriatic (ADRIATIC-C). In these cases, which are characterized by localized ocean circulation patterns driven by larger scale atmospheric dynamical forcing, the global model shows a symmetric distribution of the fluctuations whereas observations are characterized by a prevalence of warm anomalies, which are correctly described by the regional model.

Although the improvements in the statistics of the residual fluctuations are not uniform over all the considered sites, and a few counter examples are also reported in Table 4, the examples discussed above highlight the added value of using a higher resolution ocean component in describing the impact of local dynamics on shorter-time scale fluctuations.

4 Future scenarios: implications for selected impacts

In the following sections, we present relevant outcomes from the simulations performed with the ENEA-REG in terms of projected changes in ECV and EOVs; besides, we also describe the changes in occurrence and characteristics of marine heat waves in the three different analyzed scenarios.

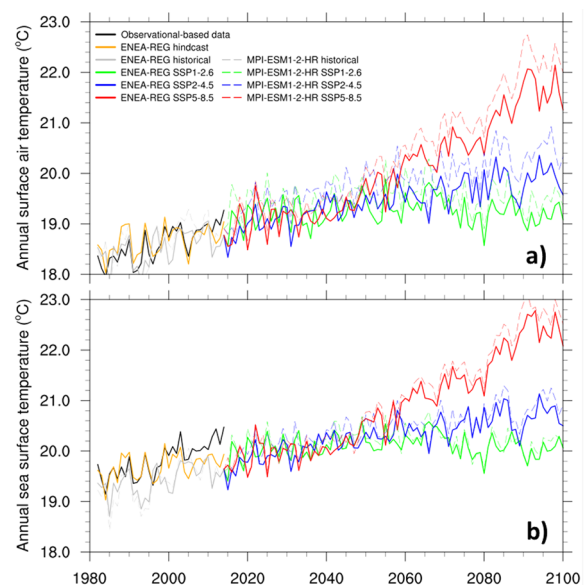


Fig. 10 Annual time series of near-surface air temperature (a) and Sea Surface temperature (b) ($^\circ\text{C}$) from the ENEA-REG scenario simulations averaged over the entire Mediterranean basin

Considering the overall behavior of the three scenarios simulations, Fig. 10 shows the temporal evolution of annual near-surface air temperature and sea surface temperature

averaged over the entire Mediterranean basin (sea only) as simulated by ENEA-REG, along with corresponding global driver simulations and observational datasets for reference.

In the historical period, the ENEA-REG hindcast simulation seems to slightly amplify the relative minimum in SST of 2004–2005 values (García-Monteiro et al 2022) after the 2003 heat wave. After this event, the oceanic component of the model exhibits a cold bias (see Fig. 10b) also present, but weaker, in 2 m temperature (Fig. 10a). This feature has been already highlighted by Ruti et al. (2016) for the first releases of Med-CORDEX coupled simulations, and, more recently, in Storto et al. (2023).

Looking at the future projections, results highlight how the different scenarios are quite close in the first half of XXI century, then they tend to diverge after 2050 with a

difference at the end of the century between SSP2-4.5 and SSP5-8.5 of around 2 °C. In addition, an overall agreement can be observed between the regional simulations and corresponding global drivers, although the downscaling experiments show a weaker magnitude of the trend in the scenarios SSP2-4.5 and SSP5-8.5 for both air surface temperature and SST, while, consistent with the global forcing, no relevant warming is simulated in the scenario SSP1-2.6.

4.1 Projected changes in relevant atmospheric ECVs

Figure 11 shows the spatial patterns of the air surface temperature change for the three scenario simulations between the end of XXI century and the historical period. Consistently with most of the globe (Tebaldi et al. 2020), the

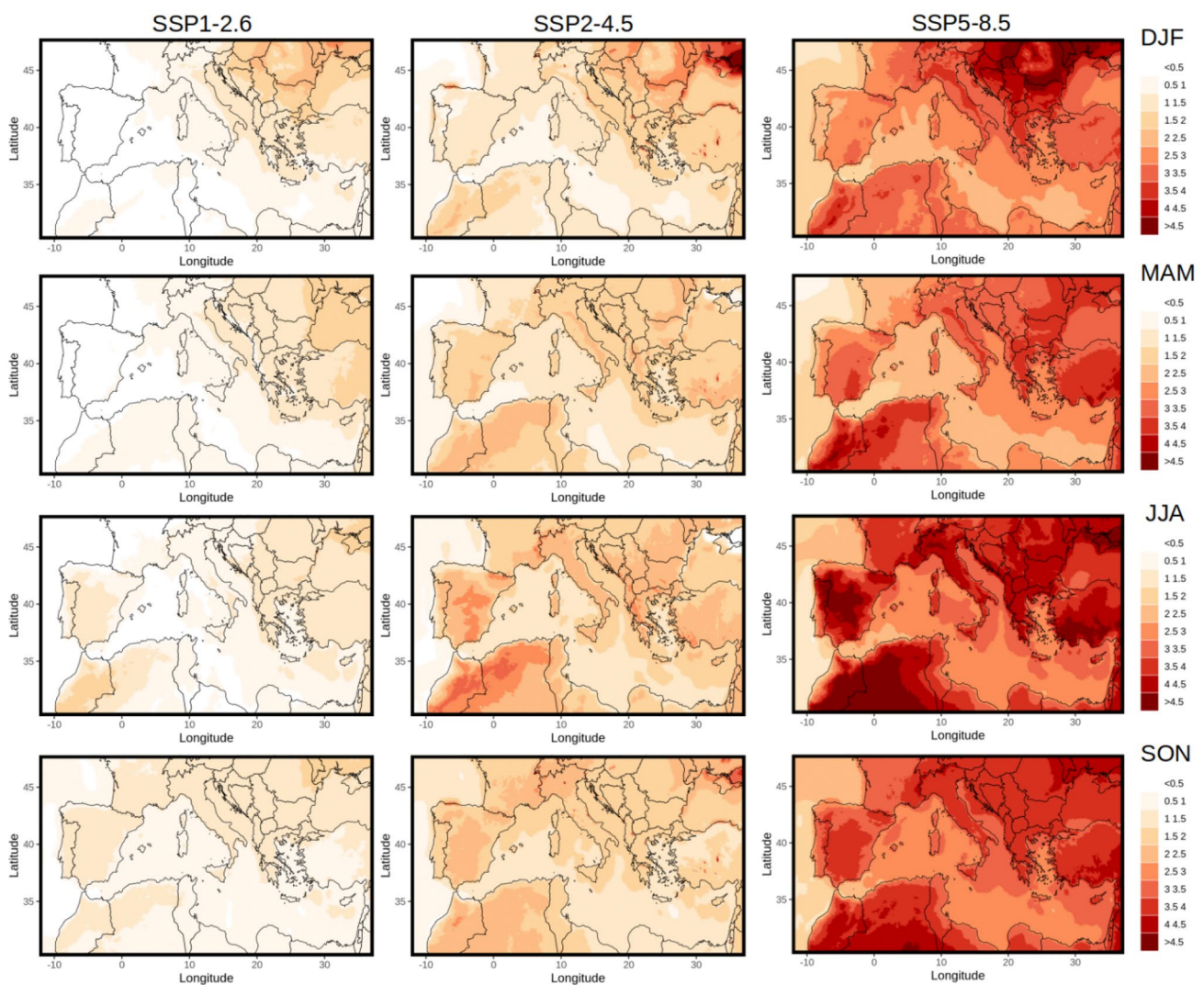


Fig. 11 Near-surface air temperature (K) projected climate change (2071–2100 minus 1985–2014) from the ENEA-REG scenario simulations: SSP1-2.6 (left column), SSP2-4.5 (central column) and SSP5-8.5 (right column). Boreal winter DJF (first row), spring MAM

(second row), summer JJA (third row), autumn SON (fourth row). Values at all grid points are significant at 10% level. Significance assessed by bootstrap procedure with 1000 repetitions

warming over the Mediterranean region is projected to be much larger over land than over the sea. Generally, the most relevant changes are experienced in the summer season under the SSP5-8.5 with projected mean warming up to 5 °C in the Iberian Peninsula and North Africa. Over Tyrrhenian Sea and in the eastern Mediterranean basin surface air temperature is projected to increase up to 2.5 °C, while in the Adriatic an increase of 4 °C is expected to be reached during SON. During winter, temperatures tend to increase mostly over Eastern Europe. The SSP2-4.5 displays a quite similar spatial patterns compared to SSP5-8.5, but with a weaker warming of about 1.5 °C, on average. Finally, according to the SSP1-2.6, in the Euro-Mediterranean domain only few areas (Eastern Europe in winter and northern Africa in summer) could experience a project warming up to 2 °C.

Looking at changes in the mean precipitation (Fig. 12), the ENEA-REG simulates a strong rainfall reduction over Mediterranean basin mainly in SSP5-8.5 and SSP2-4.5 and for all the seasons, while in the SSP1-2.6 the largest decrease in the Euro-Mediterranean region is found in SON. Besides a common pattern is observed between the three scenarios: in particular, during summer, mean precipitation tends to generally reduce, mostly in the western part of the domain and over Balkan peninsula, while during winter and partially in spring more precipitation is projected in the central and western Europe.

The above reported features for mean air surface temperature and precipitation are fully consistent to what already reported in the last IPCC report (IPCC 2022). Furthermore, considering the annual mean trends instead of the seasonal

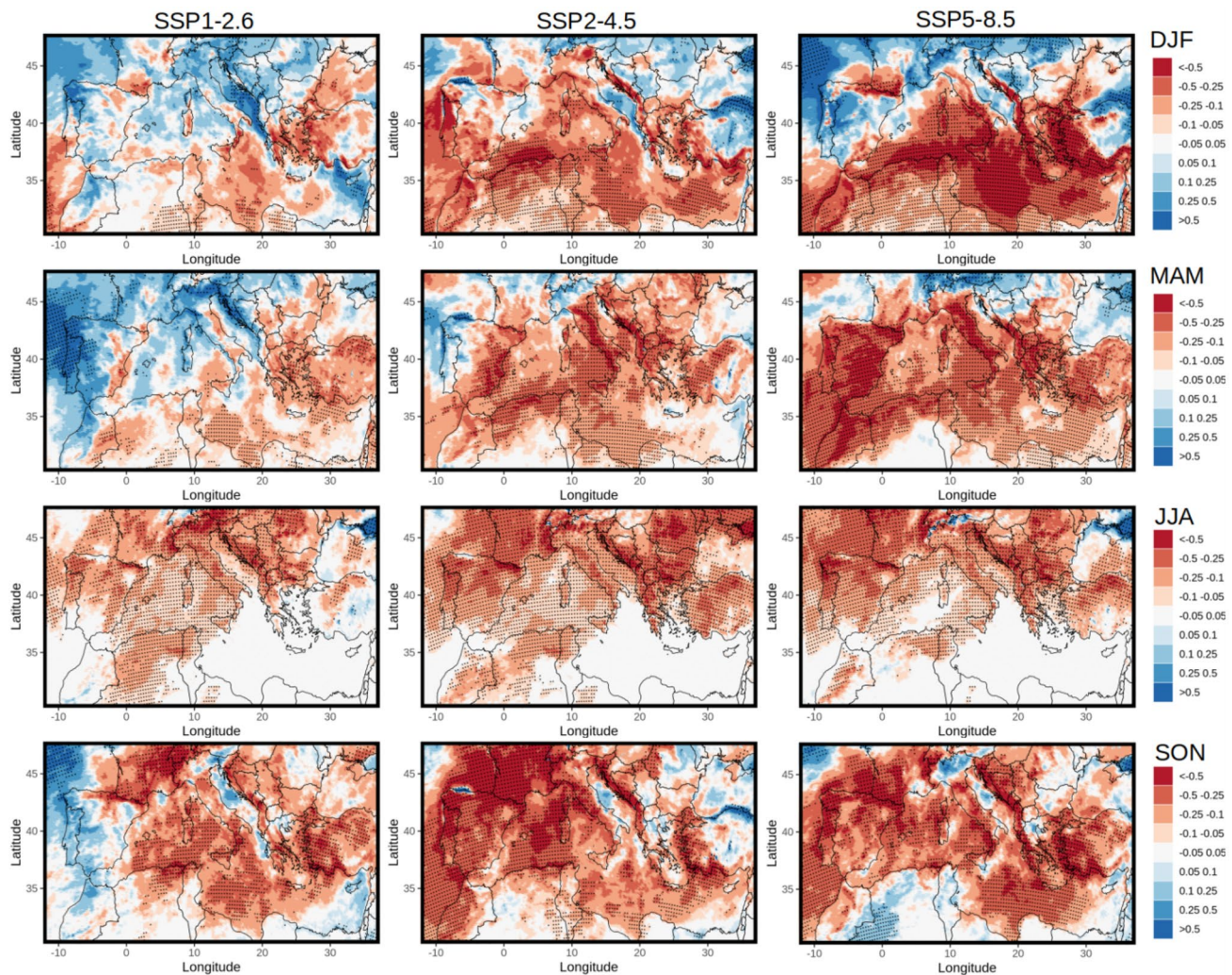


Fig. 12 Precipitation (mm d^{-1}) projected climate change (2071–2100 minus 1985–2014) from the ENEA-REG scenario simulations: SSP1-2.6 (left column), SSP2-4.5 (central column) and SSP5-8.5 (right column). Boreal winter DJF (first row), spring MAM (second row), sum-

mer JJA (third row), autumn SON (fourth row). Black dots indicate 10% level significance, assessed by bootstrap procedure with 1000 repetitions

values showed in Figs. 11 and 12, our results are fully in line to what reported by Zittis et al. (2019).

4.2 Projected changes in relevant EOVs

Looking at the oceanic component of ENEA-REG, in Tables 5 and 6 we present the changes in temperature and salinity profiles for the three scenario simulations between the end of XXI century and the historical period. We focus on two 20-year periods (2046–2065; 2081–2100) to highlight mid-term and long-term changes with respect to the reference historical simulation.

At mid-century, the average positive temperature anomalies over the whole Mediterranean basin increase with the severity of the scenario in the surface and intermediate layers, reaching a maximum of about 1 °C. Anomalies in the deepest layer are smaller, and almost independent on the scenario. Results also point out a difference between the main sub-basins, with markedly higher surface anomalies in the eastern sub-basin, and higher intermediate anomalies in the western sub-basin. The latter may reflect the downward propagation of the local surface heat surplus, but inflow of warmer Levantine Intermediate Water (LIW) from the eastern Mediterranean could also contribute. As for salinity, the

Table 5 Differences between values averaged over the period 2046–2065 of the three scenarios and the whole period (1985–2014) of the historical simulation

		Depth (m)		
		0–150	150–600	600–3500
Temperature				
MED	SSP126	0.73	0.88	0.47
	SSP245	0.85	0.97	0.45
	SSP585	1.07	1.00	0.46
WMED	SSP126	0.59	1.05	0.58
	SSP245	0.66	1.17	0.57
	SSP585	0.75	1.18	0.57
EMED	SSP126	0.81	0.79	0.40
	SSP245	0.95	0.85	0.37
	SSP585	1.25	0.89	0.39
Salinity				
MED	SSP126	– 0.11	0.19	0.17
	SSP245	– 0.10	0.18	0.13
	SSP585	– 0.14	0.14	0.13
WMED	SSP126	– 0.22	0.23	0.16
	SSP245	– 0.24	0.23	0.14
	SSP585	– 0.28	0.20	0.14
EMED	SSP126	– 0.05	0.16	0.17
	SSP245	– 0.02	0.14	0.12
	SSP585	– 0.06	0.10	0.13

Averages are computed over the whole Mediterranean Sea (MED), and over the western and eastern sub-basins (WMED and EMED)

Table 6 Differences between values averaged over period 2081–2100 of the three scenarios and the whole period (1981–2014) of the historical simulation

		Depth (m)		
		0–150	150–600	600–3500
Temperature				
MED	SSP126	0.61	0.91	0.66
	SSP245	1.05	1.11	0.61
	SSP585	2.45	2.08	0.68
WMED	SSP126	0.46	1.12	0.84
	SSP245	0.92	1.47	0.84
	SSP585	2.16	2.40	0.88
EMED	SSP126	0.70	0.78	0.55
	SSP245	1.12	0.89	0.46
	SSP585	2.62	1.89	0.56
Salinity				
MED	SSP126	– 0.15	0.08	0.18
	SSP245	– 0.27	0.06	0.15
	SSP585	– 0.06	0.22	0.16
WMED	SSP126	– 0.21	0.16	0.19
	SSP245	– 0.38	0.19	0.18
	SSP585	– 0.27	0.33	0.18
EMED	SSP126	– 0.12	0.03	0.17
	SSP245	– 0.21	– 0.01	0.13
	SSP585	0.06	0.16	0.15

Averages are computed over the whole Mediterranean Sea (MED), and over the western and eastern sub-basins (WMED and EMED)

anomalies are negative in the upper layer and positive in the others, indicating a stronger stratification of the water column.

At the end of century, temperature anomalies over the Mediterranean basin generally increase at all levels for all scenarios, except for a slight decrease in the upper layer of SSP1-2.6. The strongest increase is for the SSP5-8.5 scenario, where anomalies are more than doubled with respect to the mid-term period in the surface and intermediate layers (the maximum anomaly in the eastern upper layer reaches 2.6 °C). This is consistent with Fig. 10, which shows that, starting from 2060, the rate of increase of the basins SST becomes much stronger for this scenario. The salinity differences vary among scenarios, displaying the greatest negative values in the upper layer of the western sub-basin, indicating a growing effect of the fresher Atlantic Water (AW) inflow.

The estimate of global mean sea level change under future scenarios has been presented in the IPCC report (Fox-Kemper et al. 2021), based on about 40 CMIP6 global coupled simulations. The main contribution to the sea level change is represented by thermal expansion, that is computed as a global mean for each model. The other processes, including the melting of sea ice in the Arctic and Antarctic Oceans, the loss of mass from glaciers, the contribution of the change in

land water storage and the vertical land motion have been computed by means of specific models in dedicated inter-comparison projects.

Figure 13 shows the total sea level change, averaged over the Mediterranean basin, and computed from the AR6 models, for the three analyzed scenarios. The global projections and confidence levels are relative to the baseline period 1995–2014; total values obtained using the MPI-ESM1-2-HR and the ENEA-REG are also shown. Results highlight how both the driving global model and the regional simulations are close to the ensemble's median. Besides, sea level height increases when going from SSP1-2.6 to SSP5-8.5. The major difference with respect to the AR6 median is found at the end of the period in the most severe scenario when the MPI-ESM1-2-HR and ENEA-REG means are about 10 cm lower than the AR6.

A deeper insight into the sea level change under the three scenarios is shown in Fig. 14 where are presented sea level patterns due only to the circulation component, averaged over the last 5 years of the simulations (2096–2100) relative to the 1995–2014 historical period. In general, the patterns of the global driving model are smoother than the regional model; for instance, the east–west difference that is only slightly perceptible in the MPI-ESM1-2-HR simulations is intensified in the regional ones for all the three scenarios. While the global model is virtually uniform in the eastern area, in all scenarios the regional model shows an extensive area of negative values in the central part of the basin and positive values along the corresponding shores.

Under the most severe scenario, the maximum around the Balearic Islands ranges from about 10 cm in the global model to 30 cm in the regional ones and the negative values covering the entire Adriatic Sea in MPI-ESM1-2-HR correspond to higher values in ENEA-REG.

Due to the concentration of population in Mediterranean coastal zones, the extreme sea level heights reached along the coast represent one of the major impacts of future scenarios. Thus, we present in Fig. 15 the monthly mean values near three of the main Italian ports (Genoa, Naples, and Venice) derived from the global and regional simulations, while mean and standard deviations are in Table 7. Except for Venice under the SSP1-2.6 scenario, all the means computed for the regional model are slightly lower than for the driving GCM. Results suggest that the general increase in the variability of local sea level can result in higher extreme events in the regional simulation.

4.3 Projected impact in future scenarios: implication for heat waves

To illustrate the potential application of high-resolution SST fluctuations in the description of localized marine heatwaves for impact studies, in the following analysis we consider the SST components

$$SST_{T,R} = SST_T + SST_R \quad (6)$$

representing the combined effect of the short-term fluctuations and of the long-term tendency in determining the onset of marine heatwaves. In particular, we define heatwaves as periods during which $SST_{T,R}$ is above a certain threshold for a period longer than 5 days.

As an example, Fig. 16 shows the maximum intensity and total annual duration of marine heatwaves in the central Adriatic. Over this area, the regional climate model is expected to improve the description of temperature variability, especially during summer, when local processes in the atmosphere are more relevant, as well as during fall. The

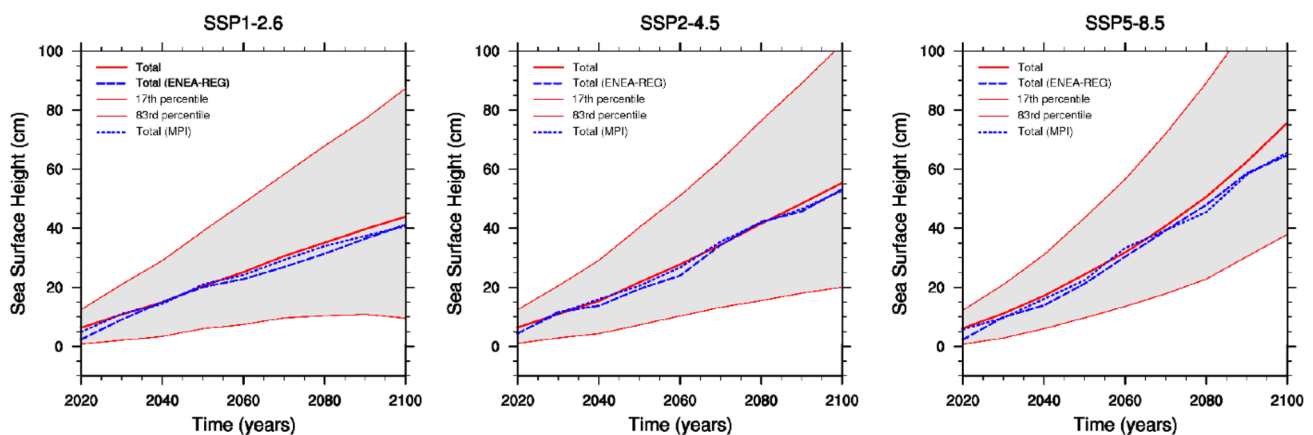


Fig. 13 Change of the average total sea level over the Mediterranean basin for the three SSP scenarios (blue curves; dotted=MPI-ESM1-2-HR; dashed=ENEA-REG). The projections are relative to a 1995–

2014 baseline. The thick red line is the median over the AR6 models and the shaded area corresponds to the 17th–83rd percentile range

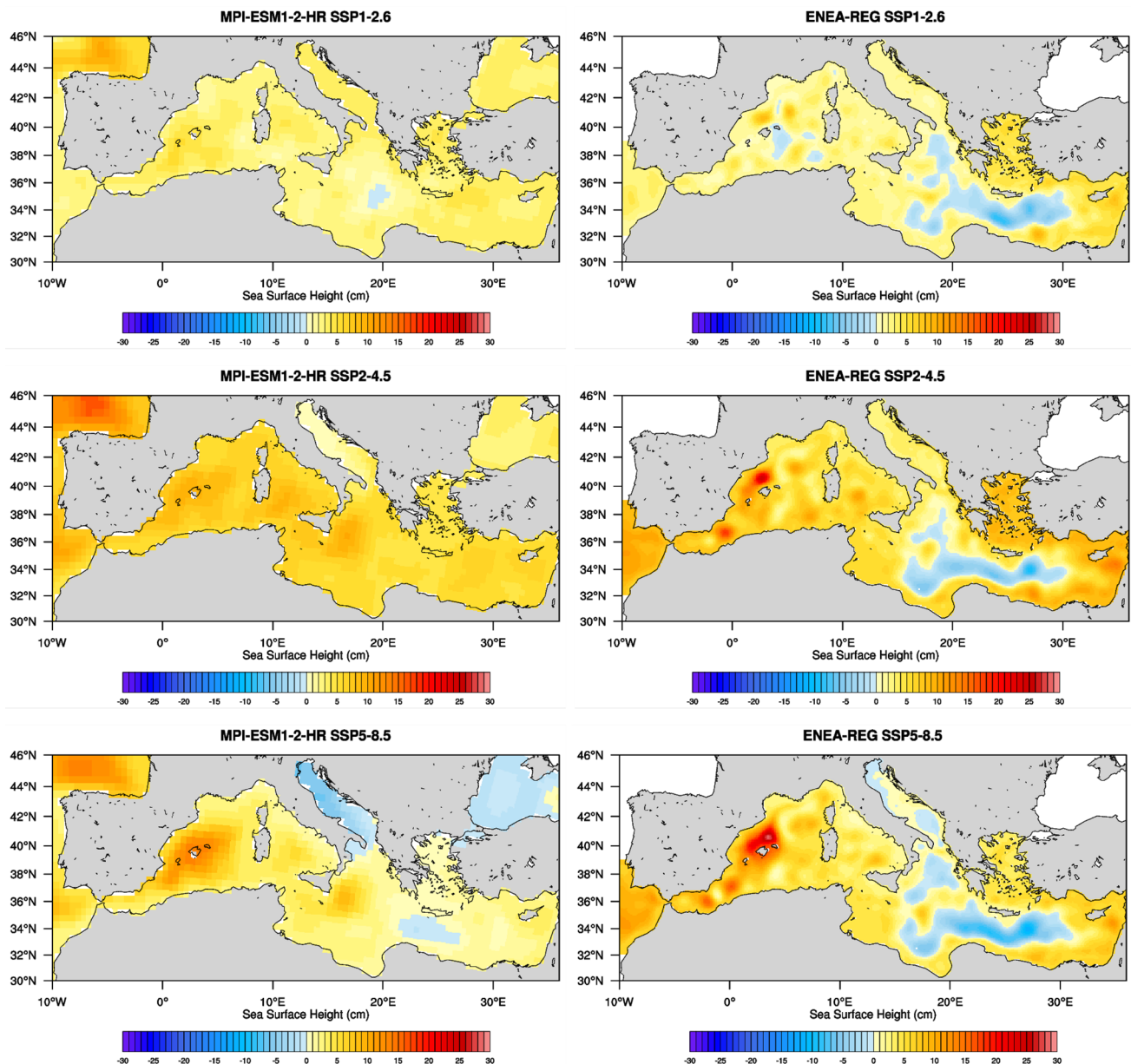


Fig. 14 Sea surface height computed averaging the last five years of the simulations respect to the average over the historical period 1995–2014. Left panels for the MPI-ESM1-2-HR model, right panels ENEA-REG simulations. Only the circulation component is considered

figure is constructed by progressively shifting the heatwave threshold from the 95-th percentile to the maximum value of the model $SST_{T,R}$ over the historical period (vertical axis). Therefore, the height of the vertical bars represents the maximum intensity of the heatwaves during each year; colors are associated to the sum of the durations of all heatwaves during the same calendar year.

The initial part of the time series, until 2014, is identical for the three scenarios as it is derived from the same historical simulation. For the following years, Fig. 16 shows the time series of marine heatwaves for the three scenarios

simulated with the regional climate model ENEA-REG (a), and with the corresponding global model driver MPI-ESM1-2-HR (b).

During the historical period, sporadic marine heatwaves appear in the time series. The intensity is approximately uniform, with a mild tendency to increase frequency between 1980 and 2014.

A key result emerging from the comparison between the three scenarios is the different behavior between SSP1-2.6 and the other two scenarios SSP2-4.5 and SSP5-8.5. In the scenario SSP1-2.6, marine heatwaves stabilize during

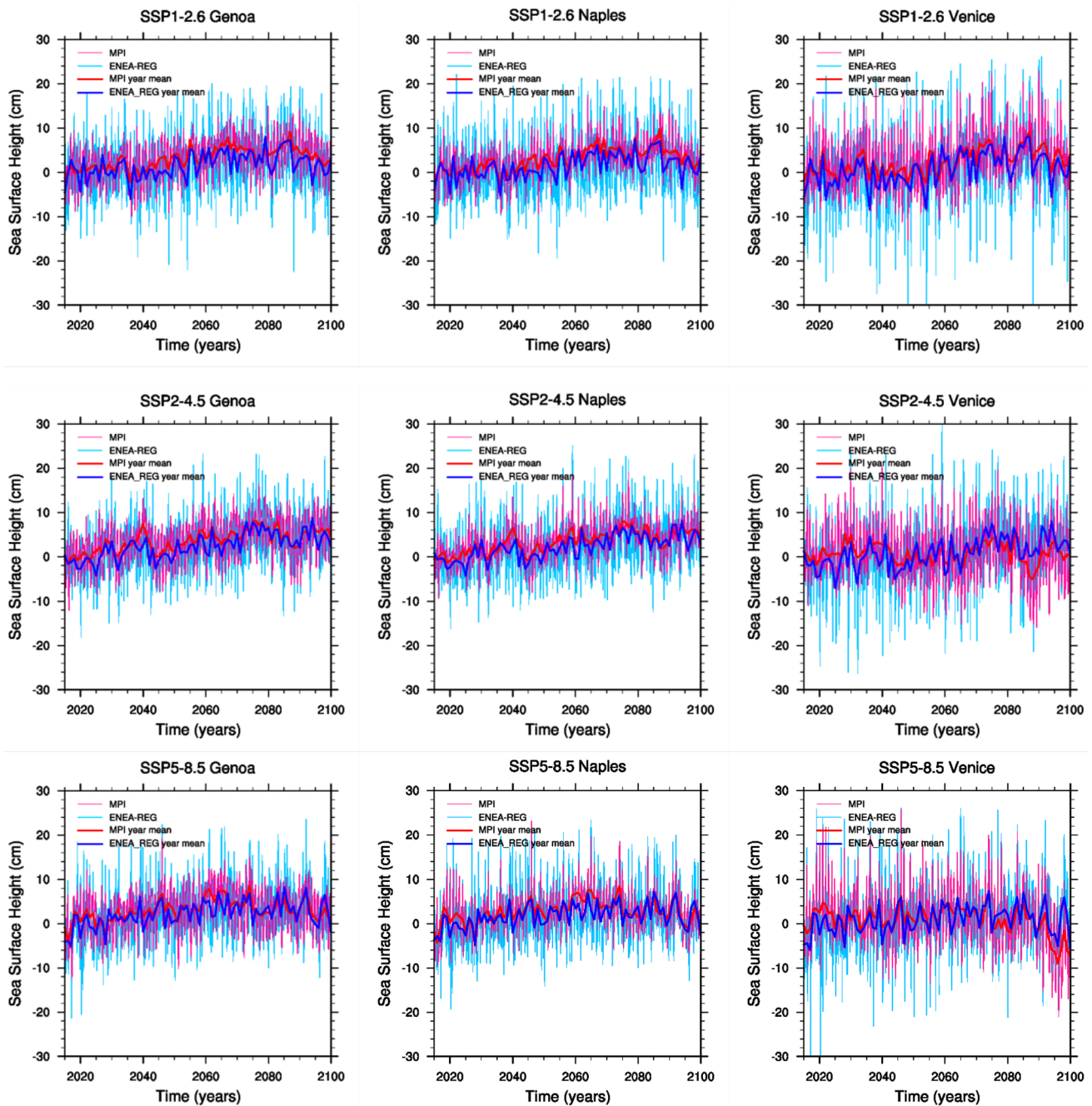


Fig. 15 Comparison of the MPI-ESM1-2-HR (MPI) and ENEA-REG sea surface height for model points near to Genoa, Naples and Venice. From the left to the right column, scenario SSP1-2.6, SSP2-4.5

and SSP5-8.5. Monthly values and yearly means are shown. Values are computed with respect to the average over the 1995–2014 historical period

the second half of the century in intensity, frequency and duration. In this scenario, the marine heatwave maximum intensity by the end of the century is comparable with the intensity detected in the historical simulation. Instead, for the scenarios SSP2-4.5 and SSP5-8.5, the intensity, frequency and duration of heatwaves continue to increase until the end of the century. Besides, in the scenario SSP5-8.5, the total annual length of marine heatwave increases from a few

days during the initial period to virtually the entire annual cycle by the end of the simulation in 2100. In other words, anomalies of up to 2 °C which are considered extreme (i.e. above the 95-th percentile) at the beginning of the century, will become so frequent to be the norm in less than a hundred years under the SSP5-8.5 scenario. Such a difference between the SSP1-2.6 and the other two scenarios occurs for all the areas listed in Table 4 (not shown).

Table 7 Comparison of sea level height mean and standard deviation for the three scenarios on model points near to Genoa, Naples, and Venice

Site	Scenario	MPI-ES-1-2-HR (cm)	ENEA-REG (cm)
GENOA	SSP1-2.6	3.1 ± 4.5	1.6 ± 6.6
	SSP2-4.5	3.6 ± 4.8	2.4 ± 6.1
	SSP5-8.5	3.0 ± 4.9	2.2 ± 6.3
VENICE	SSP1-2.6	2.4 ± 6.0	0.7 ± 8.5
	SSP2-4.5	0.7 ± 6.1	0.8 ± 7.9
	SSP5-8.5	0.9 ± 6.6	0.9 ± 7.8
NAPLES	SSP1-2.6	3.0 ± 4.0	1.5 ± 6.8
	SSP2-4.5	3.4 ± 4.0	2.2 ± 6.3
	SSP5-8.5	2.7 ± 4.3	1.8 ± 6.4

Values are computed with respect to the average over the 1995–2014 historical period

In the specific case of the central Adriatic, the global model tends to underestimate the frequency of heatwaves during the historical period and to overestimate the duration and intensity in the scenarios. Along with the improved model variability in this area, as described in Fig. 4, and the improved statistics of fluctuations reported in Table 4, this result suggests that the description of marine heatwaves may benefit from the use of higher resolution coupling, especially over enclosed sub-basins.

5 Summary and conclusions

We presented an improved version of a regional ESM designed to represent the present and future climate variability over the Euro-Mediterranean basin, a well-known hot-spot region for climate change (Giorgi 2006). The new version of the model goes in the direction of adhering to the Phase3 Med-CORDEX protocol. In particular, we have adopted the mandatory resolutions of the new protocol, for both atmosphere and ocean. The major objectives of this paper, i.e. the study of marine heatwaves and of the sea level projections in the Mediterranean, coincide with the focuses envisaged in Med-CORDEX phase 3. Thus, we believe our results can contribute to the ensemble of climate projections over the Euro-Mediterranean region.

Compared to other modeling systems developed within the Med-CORDEX initiative (e.g. Sevault et al. 2014; Reale et al. 2020; Soto-Navarro et al. 2020), we have significantly increased the spatial resolution of the atmospheric component, while the explicit formulation of a free sea surface allows to simulate sea level rise within the Mediterranean Sea (Sannino et al. 2022).

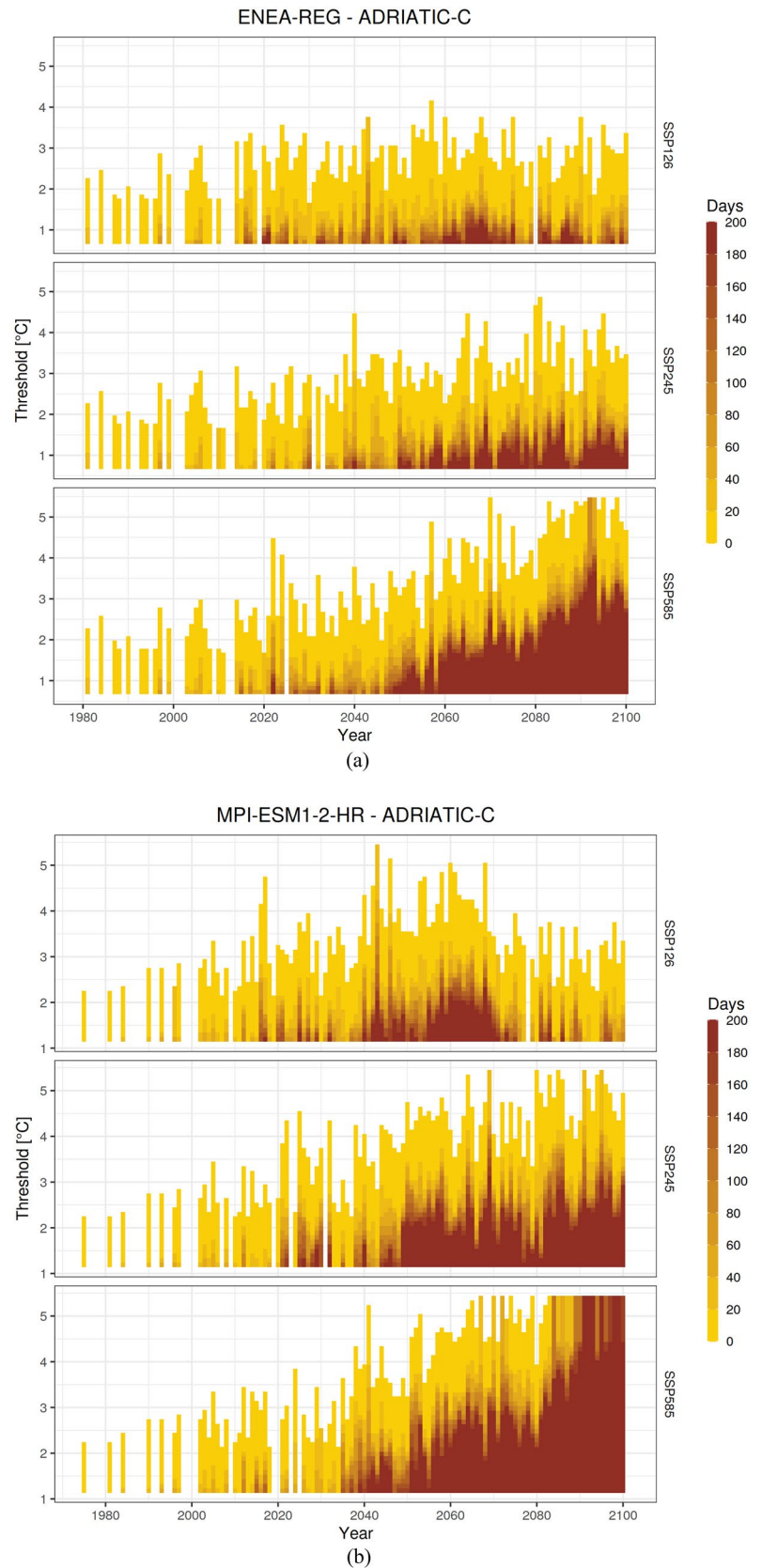
Besides, we evaluated the performances of individual model components comparing results, for the present

climate, from hindcast (i.e. ERA5-driven) and historical (i.e. GCMs-driven) simulations against the state-of-the-art of observational and reanalysis datasets. Overall, results indicated that the atmospheric component of the regional ESM simulates reasonably well the main spatio-temporal characteristics of the analyzed essential climate variables (temperature and precipitation), with precipitation not showing any relevant bias. Considering the surface air temperature, compared to the first ENEA-REG version (Anav et al. 2021) we substantially improved the performances of the hindcast simulation: in particular, the summer warm bias over the whole continental Europe (except Spain), exceeding the 4 °C at some locations, was considerably reduced. Similarly, the cold bias occurring in North-Eastern Europe during winter has noticeably decreased in magnitude.

The improved performances during summer mostly depended on the differences in the parameterization used to represent the microphysics. As detailed microphysics schemes are computationally demanding, in the original ENEA-REG version we used a bulk parameterization of cloud particles and precipitation drops; this scheme assumes an underlying shape for the hydrometeor size distribution and predicts one or more bulk quantities of the distribution (Hong et al. 2004; Morrison et al. 2009). Conversely, in the updated ENEA-REG version, we use an improved bulk microphysics scheme that predicts two moments of the hydrometeor size spectra rather than just one (Morrison et al. 2009). In our case, the switch from a single-moment to a double-moment microphysics scheme leads to a remarkable reduction in the summer dry bias and, consequently, part of the surface heat flux is converted into latent heat, reducing thus the surface warming, and, consequently, the warm summer bias. On the other side, the cold winter bias is quite common for WRF simulations on wooded and snow-covered areas of Europe; it mainly depends on the overestimation of snow depth and poor representation of the snow–atmosphere interactions, amplified by the albedo feedback (e.g., Mooney et al. 2013; García-Díez et al. 2015; Katragkou et al. 2015; Varga and Breuer 2020). The reduced winter cold bias over North-Eastern Europe can be explained by the optimization of some snow cover parameters, within the updated WRF release, which could have improved the model’s performance in simulating snow water equivalent, snow depth, and surface albedo.

At the same time, the performances of the ocean model have improved. For instance, for the surface salinity we find smaller biases with respect to the previous ENEA-REG version, while looking at the sea surface temperature, the summer warm bias (> 2 °C) in the Tyrrhenian and Sardinian Sea disappeared and the bias generally remains within ± 1 °C. The reduction of the sea surface temperature bias is related to the improvement in the atmospheric component of the system. Moreover, the use of monthly

Fig. 16 Intensity and total annual length of heatwaves for the central Adriatic as described by ENEA-REG (a) and by the global driver MPI-ESM1-2-HR. The thresholds for the identification of heatwaves are set between the 95-th percentile and the maximum value of the corresponding daily temperature anomalies w/r to the local seasonal cycle during the historical period (1980–2014). Heatwaves are defined as periods of at least 5 consecutive days with temperature anomaly above the threshold



boundary conditions, rather than climatological values in the Atlantic box, has a positive impact on the performances of the ocean component of the regional ESM.

Considering the simulated future climate, a general warming of the Mediterranean Sea with respect to the present is projected under all the scenarios in terms of both air surface temperature and SST. A stable positive trend is observed under SSP2-4.5 and SSP5-8.5, while SSP1-2.6 induces a more limited warming up to mid-century, to then reverse such tendency and stabilize around a moderate increase of about 0.7 °C for both the ocean and the atmosphere, highlighting how the inertia of the climate system is expected to anyway shadow the benefits of climate action for a few decades ahead. An overall agreement can be observed between the regional simulations and corresponding global driver, although the downscaling experiments tend to underestimate the trends.

Looking at precipitation, the ENEA-REG foresees a relevant reduction for the mean precipitation over Mediterranean basin mainly in SSP5-8.5 and SSP2-4.5, consistently to what already reported in IPCC AR6 WG1 (Fox-Kemper et al. 2021).

The Mediterranean dynamic sea level (i.e. the component due to the circulation) increases for all scenarios, more conspicuously under SSP5-8.5 and SSP2-4.5. Both spatial and temporal variability are enhanced in the regional simulations with respect to the global projections, which might have a non-negligible impact on coastal risk assessments.

Regarding the representation of marine heatwaves, we have highlighted the potential advantage of using a higher resolution ocean component in describing the impact of local dynamics on shorter-time scale fluctuations, especially over enclosed sub-basins such as the Adriatic Sea. Our results suggest that the intensity, frequency, and duration of marine heat waves will continue to increase until the end of the century for the scenarios SSP2-4.5 and SSP5-8.5, whereas for SSP1-2.6 they stabilize after the first half of the century, coherently with the overall trend. In particular, anomalies of up to 2 °C which are considered extreme (i.e. above the 95-th percentile) at the beginning of the century, will be so frequent to become the norm in less than a hundred year for the SSP5-8.5 scenario, thereby implying potential severe impacts on ecosystems, on ecosystem services and on local communities and on the broader Mediterranean economy.

Supplementary Information The online version contains supplementary material available at <https://doi.org/10.1007/s00382-023-07064-3>.

Acknowledgements We acknowledge the World Climate Research Programme, which, through its Working Group on Coupled Modelling, coordinated and promoted CMIP6. Within this we thank the CMIP6 endorsement of the High-Resolution Model Intercomparison Project (HighResMIP) and Martin Schupfner for providing additional data from the MPI-ESM. The computing resources and the related

technical support used for this work have been provided by CRESCO/ ENEA-GRID High Performance Computing infrastructure and its staff

Author contributions All authors discussed the results and contributed to the writing of the article; AA performed the simulations.

Funding Open access funding provided by Ente per le Nuove Tecnologie, l'Energia e l'Ambiente within the CRUI-CARE Agreement. This study was carried out within: ICSC Italian Research Center on High-Performance Computing, Big Data and Quantum Computing and received funding from the European Union Next-GenerationEU (National Recovery and Resilience Plan-NRRP, Mission 4, Component 2, Investment 1.4-D.D: 3138 16/12/2021, CN00000013). RETURN Extended Partnership and received funding from the European Union Next-GenerationEU (National Recovery and Resilience Plan-NRRP, Mission 4, Component 2, Investment 1.3-D.D. 1243 2/8/2022, PE0000005). CoCliCo (Coastal Climate Core Service) research project which received funding from the European Union's Horizon 2020 Research and Innovation Programme under Grant agreement No. 101003598. CAREHeat (detection and threats of marine Heat waves) project, funded by the European Space Agency (ESA, grant agreement no. 4000137121/21/I-DT).

Data availability Enquiries about data availability should be directed to the authors.

Declarations

Conflict of interest The authors of this paper have no relevant financial or non-financial interests to disclose.

Open Access This article is licensed under a Creative Commons Attribution 4.0 International License, which permits use, sharing, adaptation, distribution and reproduction in any medium or format, as long as you give appropriate credit to the original author(s) and the source, provide a link to the Creative Commons licence, and indicate if changes were made. The images or other third party material in this article are included in the article's Creative Commons licence, unless indicated otherwise in a credit line to the material. If material is not included in the article's Creative Commons licence and your intended use is not permitted by statutory regulation or exceeds the permitted use, you will need to obtain permission directly from the copyright holder. To view a copy of this licence, visit <http://creativecommons.org/licenses/by/4.0/>.

References

- Allen MR, Smith LA (1997) Optimal filtering in singular spectrum analysis. *Phys Lett A* 234(6):419–428
- Anav A, Friedlingstein P, Kidston M, Bopp L, Ciais P, Cox P, Jones C, Jung M, Myneni R, Zhu Z (2013) Evaluating the land and ocean components of the global carbon cycle in the CMIP5 earth system models. *J Clim* 26(18):6801–6843
- Anav A, Carillo A, Palma M, Struglia MV, Turuncoglu UU, Sannino G (2021) The ENEA-REG system (v1.0), a multi-component regional Earth system model: sensitivity to different atmospheric components over the Med-CORDEX (coordinated regional climate downscaling experiment) region. *Geosci Model Dev* 14(7):4159–4185
- Artale V, Calmanti S, Carillo A, Dell'Aquila A, Herrmann M, Pisacane G, Ruti PM, Sannino G, Struglia MV, Giorgi F (2010) An atmosphere–ocean regional climate model for the Mediterranean area: assessment of a present climate simulation. *Clim Dyn* 35:721–740

- Bruyère CL, Done JM, Holland GJ, Fredrick S (2014) Bias corrections of global models for regional climate simulations of high-impact weather. *Clim Dyn* 43:1847–1856
- Campin J-M, Adcroft A, Hill C, Marshall J (2004) Conservation of properties in a free-surface model. *Ocean Model* 6(3–4):221–244
- Cardoso RM, Soares PM (2022) Is there added value in the EURO-CORDEX hindcast temperature simulations? Assessing the added value using climate distributions in Europe. *Int J Climatol* 42(7):4024–4039
- Carillo A, Sannino G, Artale V, Ruti P, Calmanti S, Dell'Aquila A (2012) Steric sea level rise over the Mediterranean Sea: present climate and scenario simulations. *Clim Dyn* 39:2167–2184
- Christensen JH, Christensen OB (2007) A summary of the PRUDENCE model projections of changes in European climate by the end of this century. *Clim Change* 81:7–30
- Ciais P, Reichstein M, Viovy N, Granier A, Ogee J, Allard V, Aubinet M, Buchmann N, Bernhofer C, Carrara A (2005) Europe-wide reduction in primary productivity caused by the heat and drought in 2003. *Nature* 437(7058):529–533
- Cos J, Doblas-Reyes F, Jury M, Marcos R, Bretonnière P-A, Samsó M (2022) The Mediterranean climate change hotspot in the CMIP5 and CMIP6 projections. *Earth Syst Dynam* 13:321–340. <https://doi.org/10.5194/esd-13-321-2022>
- Darmaraki S, Somot S, Sevault F, Nabat P, Cabos Narvaez WD, Cavicchia L, Djurdjevic V, Li L, Sannino G, Sein DV (2019) Future evolution of marine heatwaves in the Mediterranean Sea. *Clim Dyn* 53:1371–1392
- Doblas-Reyes F, Sorensson A, Almazroui M, Dosio A, Gutowski W, Haarsma R, Hamdi R, Hewitson B, Kwon W-T, Lamptey B (2021) Linking global to regional climate change climate change. 2021: the physical science basis. Contribution of working group I to the sixth assessment report of the intergovernmental panel on climate change. Cambridge University Press
- Dosio A (2016) Projections of climate change indices of temperature and precipitation from an ensemble of bias-adjusted high-resolution EURO-CORDEX regional climate models. *J Geophys Res Atmos* 121(10):5488–5511
- Drobinski P, Silva ND, Panthou G, Bastin S, Muller C, Ahrens B, Borga M, Conte D, Fossier G, Giorgi F (2018) Scaling precipitation extremes with temperature in the Mediterranean: past climate assessment and projection in anthropogenic scenarios. *Clim Dyn* 51:1237–1257
- Dubois C, Somot S, Calmanti S, Carillo A, Déqué M, Dell'Aquila A, Elizalde A, Gualdi S, Jacob D, L'Hévéder B, Li L, Oddo P, Sannino G, Scoccimarro E, Sevault F (2012) Future projections of the surface heat and water budgets of the Mediterranean Sea in an ensemble of coupled atmosphere-ocean regional climate models. *Clim Dyn* 39:1859–1884. <https://doi.org/10.1007/s00382-011-1261-4>
- Eyring V, Bony S, Meehl GA, Senior CA, Stevens B, Stouffer RJ, Taylor KE (2016) Overview of the coupled model intercomparison project phase 6 (CMIP6) experimental design and organization. *Geosci Model Dev* 9(5):1937–1958
- Fantini A, Raffaele F, Torma C, Bacer S, Coppola E, Giorgi F, Ahrens B, Dubois C, Sanchez E, Verdecchia M (2018) Assessment of multiple daily precipitation statistics in ERA-Interim driven Med-CORDEX and EURO-CORDEX experiments against high resolution observations. *Clim Dyn* 51:877–900
- Fox-Kemper B, Menemenlis D (2008) Can large eddy simulation techniques improve mesoscale ocean models? Washington DC Am Geophys Union Geophys Monogr Ser 177:319–337
- Fox-Kemper B et al (2021) Ocean, cryosphere and sea level change. In: Masson-Delmotte V et al (eds) *Climate change 2021: the physical science basis*. Cambridge University Press
- García-Díez M, Fernández J, Vautard R (2015) An RCM multi-physics ensemble over Europe: multi-variable evaluation to avoid error compensation. *Clim Dyn* 45:3141–3156
- García-Monteiro S, Sobrino J, Julien Y, Sòria G, Skokovic D (2022) Surface Temperature trends in the Mediterranean Sea from MODIS data during years 2003–2019. *Reg Stud Mar Sci* 49:102086
- GCOS: The Global observing system for climate: Implementation needs, pp. 1–325 (2016) (available at <https://unfccc.int>)
- Giorgi F (2006) Climate change hot-spots. *Geophys Res Lett*. <https://doi.org/10.1029/2006GL025734>
- Giorgi F, Gutowski WJ Jr (2015) Regional dynamical downscaling and the CORDEX initiative. *Annu Rev Environ Resour* 40:467–490
- Gleckler PJ, Taylor KE, Doutriaux C (2008) Performance metrics for climate models. *J Geophys Res Atmos*. <https://doi.org/10.1029/2007JD008972>
- Gualdi S, Somot S, Li L, Artale V, Adani M, Bellucci A, Braun A, Calmanti S, Carillo A, Dell'Aquila A (2013) The CIRCE simulations: regional climate change projections with realistic representation of the Mediterranean Sea. *Bull Am Meteor Soc* 94(1):65–81
- Gutiérrez JM, Jones R, Narisma G (2021) IPCC interactive Atlas. *Climate change 2021: the physical science basis contribution of working group I to the sixth assessment report of the intergovernmental panel on climate change*. Cambridge University Press, Cambridge
- Gutjahr O, Putrasahan D, Lohmann K, Jungclaus JH, von Storch J-S, Brüggemann N, Haak H, Stössel A (2019) Max planck institute earth system model (MPI-ESM1.2) for the high-resolution model intercomparison project (HighResMIP). *Geosci Model Dev* 12(7):3241–3281
- Hagemann S, Dümenil L (1997) A parametrization of the lateral water-flow for the global scale. *Clim Dyn* 14:17–31
- Hagemann S, Gates LD (2001) Validation of the hydrological cycle of ECMWF and NCEP reanalyses using the MPI hydrological discharge model. *J Geophys Res Atmos* 106(D2):1503–1510
- Heikkilä U, Sandvik A, Sorteberg A (2011) Dynamical downscaling of ERA-40 in complex terrain using the WRF regional climate model. *Clim Dyn* 37:1551–1564
- Hersbach H, Bell B, Berrisford P, Hirahara S, Horányi A, Muñoz-Sabater J, Nicolas J, Peubey C, Radu R, Schepers D (2020) The ERA5 global reanalysis. *Q J R Meteorol Soc* 146(730):1999–2049
- Hobday AJ, Alexander LV, Perkins SE, Smale DA, Straub SC, Oliver EC, Benthuisen JA, Burrows MT, Donat MG, Feng M (2016) A hierarchical approach to defining marine heatwaves. *Prog Oceanogr* 141:227–238
- Hong S-Y, Dudhia J, Chen S-H (2004) A revised approach to ice microphysical processes for the bulk parameterization of clouds and precipitation. *Mon Weather Rev* 132(1):103–120
- IPCC W (2022) Sixth assessment report, Working Group I—The physical science basis. Regional fact sheet—Europe. Intergovernmental Panel on Climate Change
- Jacob D, Petersen J, Eggert B, Alias A, Christensen OB, Bouwer LM, Braun A, Colette A, Déqué M, Georgievski G (2014) EURO-CORDEX: new high-resolution climate change projections for European impact research. *Reg Environ Change* 14:563–578
- Janjić ZI (1994) The step-mountain eta coordinate model: Further developments of the convection, viscous sublayer, and turbulence closure schemes. *Mon Weather Rev* 122(5):927–945
- Katragkou E, García-Díez M, Vautard R, Sobolowski S, Zanis P, Alexandri G, Cardoso RM, Colette A, Fernandez J, Gobiet A, Goergen K, Karacostas T, Knist S, Mayer S, Soares PMM, Pytharoulis I, Tegoulis I, Tsikerdekis A, Jacob D (2015) Regional climate hindcast simulations within EURO-CORDEX: evaluation of a WRF multi-physics ensemble. *Geosci Model Dev* 8:603–618. <https://doi.org/10.5194/gmd-8-603-2015>

- Kotlarski S, Keuler K, Christensen OB, Colette A, Déqué M, Gobiet A, Goergen K, Jacob D, Lüthi D, Van Meijgaard E (2014) Regional climate modeling on European scales: a joint standard evaluation of the EURO-CORDEX RCM ensemble. *Geosci Model Dev* 7(4):1297–1333
- Kourafalou V, Barbopoulos K (2003) High resolution simulations on the North Aegean Sea seasonal circulation. *Ann Geophys* 21:251–265. <https://doi.org/10.5194/angeo-21-251-2003>
- Lebeaupin Brossier C, Bastin S, Béranger K, Drobinski P (2015) Regional mesoscale air–sea coupling impacts and extreme meteorological events role on the Mediterranean Sea water budget. *Clim Dyn* 44:1029–1051
- Leith CE (1968) Diffusion approximation for two-dimensional turbulence. *Phys Fluids* 11:671–673
- Marshall J, Adcroft A, Hill C, Perelman L, Heisey C (1997) A finite-volume, incompressible Navier Stokes model for studies of the ocean on parallel computers. *J Geophys Res Oceans* 102(C3):5753–5766
- Michetti M, Gualtieri M, Anav A, Adani M, Benassi B, Dalmastrì C, D’Elia I, Piersanti A, Sannino G, Zanini G (2022) Climate change and air pollution: translating their interplay into present and future mortality risk for Rome and Milan municipalities. *Sci Total Environ* 830:154680
- Millot C, Taupier-Letage I (2005) Circulation in the Mediterranean sea. *The Mediterranean sea*. Springer, pp 29–66
- Mohamed B, Abdallah AM, Alam El-Din K, Nagy H, Shaltout M (2019) Inter-annual variability and trends of sea level and sea surface temperature in the Mediterranean Sea over the last 25 years. *Pure Appl Geophys* 176:3787–3810
- Mooney P, Mulligan F, Fealy R (2013) Evaluation of the sensitivity of the weather research and forecasting model to parameterization schemes for regional climates of Europe over the period 1990–95. *J Clim* 26(3):1002–1017
- Morrison H, Thompson G, Tatarskii V (2009) Impact of cloud microphysics on the development of trailing stratiform precipitation in a simulated squall line: comparison of one- and two-moment schemes. *Mon Weather Rev* 137(3):991–1007
- Müller WA, Jungclaus JH, Mauritsen T, Baehr J, Bittner M, Budich R, Bunzel F, Esch M, Ghosh R, Haak H (2018) A higher-resolution version of the max planck institute earth system model (MPI-ESM1.2-HR). *J Adv Model Earth Syst* 10(7):1383–1413
- O’Neill BC, Tebaldi C, Van Vuuren DP, Eyring V, Friedlingstein P, Hurtt G, Knutti R, Kriegler E, Lamarque J-F, Lowe J (2016) The scenario model intercomparison project (ScenarioMIP) for CMIP6. *Geosci Model Dev* 9(9):3461–3482
- Pagès R, Baklouti M, Barrier N, Ayache M, Sevault F, Somot S, Moutin T (2020) Projected effects of climate-induced changes in hydrodynamics on the biogeochemistry of the Mediterranean Sea under the RCP 8.5 regional climate scenario. *Front Marine Sci* 7:563615
- Palma M, Iacono R, Sannino G, Bargagli A, Carillo A, Fekete BM, Lombardi E, Napolitano E, Pisacane G, Struglia MV (2020) Short-term, linear, and non-linear local effects of the tides on the surface dynamics in a new, high-resolution model of the Mediterranean Sea circulation. *Ocean Dyn* 70:935–963
- Parras-Berrocal IM, Vazquez R, Cabos W, Sein D, Mañanes R, Perez-Sanz J, Izquierdo A (2020) The climate change signal in the Mediterranean Sea in a regionally coupled atmosphere–ocean model. *Ocean Sci* 16:743–765. <https://doi.org/10.5194/os-16-743-2020>
- Pavlidis V, Katragkou E, Prein A, Georgoulas AK, Kartsios S, Zanis P, Karacostas T (2020) Investigating the sensitivity to resolving aerosol interactions in downscaling regional model experiments with WRFv3.8.1 over Europe. *Geosci Model Dev* 13(6):2511–2532
- Pinardi N, Masetti E (2000) Variability of the large scale general circulation of the Mediterranean Sea from observations and modelling: a review. *Palaeogeogr Palaeoclimatol Palaeoecol* 158(3–4):153–173
- Pinardi N, Zavatarelli M, Adani M, Coppini G, Fratianni C, Oddo P, Simoncelli S, Tonani M, Lyubartsev V, Dobricic S (2015) Mediterranean Sea large-scale low-frequency ocean variability and water mass formation rates from 1987 to 2007: a retrospective analysis. *Prog Oceanogr* 132:318–332
- Ranasinghe R, Ruane AC, Vautard R, Arnell N, Coppola E, Cruz FA, Dessai S, Saiful Islam A, Rahimi M, Carrascal DR (2021) Climate change information for regional impact and for risk assessment. *Climate change 2021: the physical science basis*. Contribution of Working Group I to the Sixth Assessment Report of the Intergovernmental Panel on Climate Change. Cambridge University Press, Cambridge, pp 1767–1926
- Reale M, Giorgi F, Solidoro C, Di Biagio V, Di Sante F, Mariotti L, Farneti R, Sannino G (2020) The regional Earth system model RegCM-ES: evaluation of the Mediterranean climate and marine biogeochemistry. *J Adv Model Earth Syst* 12(9):e2019MS001812
- Reale M, Cossarini G, Lazzari P, Lovato T, Bolzon G, Masina S, Solidoro C, Salon S (2022a) Acidification, deoxygenation, and nutrient and biomass declines in a warming Mediterranean Sea. *Biogeosciences* 19(17):4035–4065
- Reale M, Narvaez WC, Cavicchia L et al (2022b) Future projections of mediterranean cyclone characteristics using the Med-CORDEX ensemble of coupled regional climate system models. *Clim Dyn* 58:2501–2524. <https://doi.org/10.1007/s00382-021-06018-x>
- Richon C, Dutay J-C, Bopp L, Le Vu B, Orr JC, Somot S, Dulac F (2019) Biogeochemical response of the Mediterranean Sea to the transient SRES-A2 climate change scenario. *Biogeosciences* 16(1):135–165
- Rio M-H, Pascual A, Poulain P-M, Menna M, Barceló B, Tintoré J (2014) Computation of a new mean dynamic topography for the Mediterranean Sea from model outputs, altimeter measurements and oceanographic in situ data. *Ocean Sci* 10(4):731–744
- Ruiz S, Gomis D, Sotillo MG, Josey SA (2008) Characterization of surface heat fluxes in the Mediterranean Sea from a 44-year high-resolution atmospheric data set. *Global Planet Change* 63(2–3):258–274
- Ruti PM, Somot S, Giorgi F, Dubois C, Flaounas E, Obermann A, Dell’Aquila A, Pisacane G, Harzallah A, Lombardi E (2016) MED-CORDEX initiative for Mediterranean climate studies. *Bull Am Meteor Soc* 97(7):1187–1208
- Sannino G, Carillo A, Iacono R, Napolitano E, Palma M, Pisacane G, Struglia M (2022) Modelling present and future climate in the Mediterranean Sea: a focus on sea-level change. *Clim Dyn* 59(1–2):357–391
- Scherrer SC (2011) Present-day interannual variability of surface climate in CMIP3 models and its relation to future warming. *Int J Climatol* 31(10):1518–1529
- Sevault F, Somot S, Alias A, Dubois C, Lebeaupin-Brossier C, Nabat P, Adloff F, Déqué M, Decharme B (2014) A fully coupled Mediterranean regional climate system model: design and evaluation of the ocean component for the 1980–2012 period. *Tellus A* 66(1):23967
- Skamarock WC, Klemp JB (2008) A time-split nonhydrostatic atmospheric model for weather research and forecasting applications. *J Comput Phys* 227(7):3465–3485
- Somot S, Sevault F, Déqué M, Crépon M (2008) 21st century climate change scenario for the Mediterranean using a coupled atmosphere–ocean regional climate model. *Global Planet Change* 63(2–3):112–126
- Somot S, Ruti P, Ahrens B, Coppola E, Jordà G, Sannino G, Solmon F (2018) Editorial for the Med-CORDEX special issue. *Clim Dyn* 51:771–777
- Soto-Navarro J, Jordà G, Amores A, Cabos W, Somot S, Sevault F, Macías D, Djurdjevic V, Sannino G, Li L, Sein D (2020) Evolution of Mediterranean Sea water properties under climate change

- scenarios in the Med-CORDEX ensemble. *Clim Dyn* 54:2135–2165. <https://doi.org/10.1007/s00382-019-05105-4>
- Storto A, Hesham Essa Y, de Toma V, Anav A, Sannino G, Santoleri R, Yang C (2023) MESMAR v1: a new regional coupled climate model for downscaling, predictability, and data assimilation studies in the Mediterranean region. *Geosci Model Dev* 16(16):4811–4833. <https://doi.org/10.5194/gmd-16-4811-2023>
- Taranu IS, Somot S, Alias A, Boé J, Delire C (2023) Mechanisms behind large-scale inconsistencies between regional and global climate model-based projections over Europe. *Clim Dyn* 60(11–12):3813–3838
- Tebaldi C, Debeire K, Eyring V, Fischer E, Fyfe J, Friedlingstein P, Knutti R, Lowe J, O'Neill B, Sanderson B (2020) Climate model projections from the scenario model intercomparison project (ScenarioMIP) of CMIP6. *Earth Syst Dyn* 12:253–293
- Tuel A, Eltahir EA (2020) Why is the Mediterranean a climate change hot spot? *J Clim* 33(14):5829–5843
- Turuncoglu UU (2019) Toward modular in situ visualization in Earth system models: the regional modeling system RegESM 1.1. *Geosci Model Dev* 12(1):233–259
- Varga ÁJ, Breuer H (2020) Sensitivity of simulated temperature, precipitation, and global radiation to different WRF configurations over the Carpathian Basin for regional climate applications. *Clim Dyn* 55(9–10):2849–2866
- Wilks DS (2011) *Statistical methods in the atmospheric sciences*, vol 100. Academic Press
- Zittis G, Hadjinicolaou P, Klangidou M, Proestos Y, Lelieveld J (2019) A multi-model, multi-scenario, and multi-domain analysis of regional climate projections for the Mediterranean. *Reg Environ Change* 19(8):2621–2635
- Zuo H, Balmaseda MA, Tietsche S, Mogensen K, Mayer M (2019) The ECMWF operational ensemble reanalysis–analysis system for ocean and sea ice: a description of the system and assessment. *Ocean Sci* 15(3):779–808

Publisher's Note Springer Nature remains neutral with regard to jurisdictional claims in published maps and institutional affiliations.